DEPLOYMENT OF A 27.5 KHZ LINK USING NON-COHERENT SPACE TIME BLOCK CODED FREQUENCY SHIFT KEYING

by

Surinder Singh

Submitted in partial fulfillment of the requirements
for the degree of Master of Applied Science

at

Dalhousie University
Halifax, Nova Scotia
June 2020

Dedicated to my Family

Table of Contents

List of Tables

List of Figures

Abstract

The contents of this thesis explore the challenge of implementing a high-speed and reliable acoustic communication link in shallow water conditions and high-flow environments, in which highly varying propagation conditions are induced. The variability of the underwater acoustic channel is described with respect to signal attenuation, distortion due to multi-path and fading, and a link budget is calculated based on hardware parameters. These characteristics are implemented in a software model to represent a realistic ocean environment for in-lab algorithm design. The process for designing a simple, non-coherent, multiple input-multiple output (MIMO) communication system combined with frequency shift keying (FSK) to achieve robust performances are discussed. Robustness is achieved through the implementation of a space time block code. The transmitter for a software defined acoustic modem is implemented. Specifically, the transmitter digital signal processing on a hardware platform, as well as a multiple-element transmit front-end are designed and tested in the lab before being deployed at sea. Two sea trials are run: one Halifax's North West Arm in a shallow environment, and a second in the Bay of Fundy.

Two modes of operation are tested at sea: a high throughput coherent system relying on phase shift keying, as well as a low-throughput design relying on MIMO-FSK. The results of the communication algorithms demonstrate successful communication for distances up to 1 km validated through sea trial. The performance of the STBC in a real channel is evaluated and effect of the spatial correlation between the MIMO channels are discussed.

Acknowledgements

I would like to express my sincere appreciation and gratitude to my supervisor, Dr. Jean-Francois Bousquet, for his invaluable guidance, patience, and expertise throughout the writing of this thesis. Dr. Jean-Francois Bousquet, is the best Professor anyone can get for their studies. Working with J-F, (we call him J-F with respect and love) was personally, professionally and academically enriching experience that I will remember till the last day of my life.

I would like to thank my colleagues at the UW-STREAM research lab, managed by Dr. Bousquet, for providing a friendly and supportive research environment. It has been the best few years of my life and my colleagues helped me built these strong bonds that will last forever.

Finally, I would express my love and appreciation for the support of my parents, my family and my friends for continually motivating me. The love you gave and continue to give is the source of my inspiration. This work would not have been possible without your support and encouragement.

Chapter 1

Introduction

1.1 Background

Underwater communications is very important to enable civilian and military application such as sensor networks, offshore exploration, pollution monitoring and underwater surveillance [2]. However, laying down fiber cables on seabed is hugely expensive task; also the electromagnetic waves does not propagate well under the surface of ocean [3]. Hence, underwater communications using acoustic waves provides a clear advantage over optical waves and electromagnetic waves underwater. Having said that, the Underwater Acoustic Channel (UWAC) is one of the most difficult environment to work with. Many varying parameters such as multi-path propagation, attenuation due to absorption, sensitivity to various moving objects in the propagation media and flow noise in heavy flow environment are a few to mention. As such, researchers have been exploring various modulation schemes combined with advanced signal processing techniques to mitigate the effect of the distortion.

A study of modems available commercially provides a good benchmark for the specifications of the system. A thorough study about the various types of modems has been carried out in [1] and in [4]. In particular, three modems were tested in a lake environment in [1], at a distance of 74 metres. It was found that the AquaSeNT was the most robust, as it focused on reaching longer distances, at the expense of precision. The LinkQuest was found to be the most accurate and precise, but had issues communicating in short channels (large delay spread), and would occasionally produce erroneous measurements. Benthos had a balance between communication success as well as precision and accuracy. Similarly, the field tests of the NILUS MK 2 node in multihop underwater acoustic networks were performed in [4], which produces a satisfactory performance in shallow and open waters.

Table 1.1 provides a brief summary of commercially available modems. As described in [1], the Benthos and LinkQuest modems achieved 100 % reliability over 50 tests. Further research of underwater modems as covered in [4] provides information about the industry leaders in this area. EvoLogics, Develogic, SubNero, and Teledyne-Benthos are the primary

Spec	AquaSeNT	Benthos	LinkQuest	Develogic HAM	EvoLogics WiSE	SubNero
Modulation Scheme	OFDM	MFSK	DSSS	OFDM	Sweep-Spread carrier	OFDM + FH-BFSK
Freq(KHz)	14-10	9-14	26.77-44.62	6	26 or 63	27
Max. Data Rate (kb/s)	9	3.6	38,400	10	13.9 or 31.2	10
Maximum Rated Depth (Km)	7	2-6	1.2 - 1.5	23	3.5 or 1	3

Table 1.1: Commercially available modems [1]

manufacturers. Of these, they compared modems from each company except Benthos, on top of a very large number of academic modems from different universities.

It is important to understand that most of the claims regarding data rates mentioned in Table 1.1 are generally in ideal conditions. The variability of the channel impairments in both spatial and temporal domains adds to the complexity of designing a reliable underwater communication system. Physical parameters such as salinity of water, pressure, temperature, varying flow changes the sound speed profile of the signal. Additionally, the intensity of wind and direction creates surface roughness which further changes the path lengths of a ray travelling from transmitter to receiver. Due to the above mentioned phenomenon and many other random variables like shallowness of the sea and effect of side walls in the water column result in time-varying, a fading channel that is also subject to a large delay spread. Therefore, designing a reliable communication link can only be realized by taking all these impairments into consideration. The claims in Table 1.1 cannot be fulfilled in all of the different condition if the device is not adaptable or re-configurable.

Software-Defined Acoustic Modems (SDAMs) is an acoustic communication system where components that have been traditionally implemented in hardware (e.g. mixers, filters, amplifiers, modulators/demodulators, detectors, etc.) are instead implemented by means of software on a personal computer or embedded system. While the concept of SDAMs are not new, the rapidly evolving capabilities of digital electronics render practical many processes which were once only theoretically possible. A basic SDAM system consists of a digital signal processor preceded by a flexible analog front-end, preceded by some form of acoustic front end. Significant amounts of signal processing are handed over to the general-purpose processor, rather than being done in special-purpose hardware (electronic circuits). Such a design produces a modem which can receive and transmit widely different communications protocols based solely on the software used.

Most of the platforms available in the market are not capable to operate in various underwater acoustic channels. There is no “one fits all” solution available in the market.

Hence, SDAMs can fill in the gap left by the rigid systems currently available. SDAMs can be flexible, adjustable and re-configurable based on the type of acoustic channel and environment they are deployed in.

In [4], the various SDAMs are reviewed with focus on the NILUS MK-2 sensor node deployment and measurements. Specifically, in [4], a review of existing literature is produced and focuses on SDAMs for underwater communications and networking, considering past and ongoing academic efforts, as well as industrial developments. Given the fact that flexible and adaptive acoustic modems that are re-programmable/re-configurable at all layers of the communication stack, either by a user or by means of autonomous decisions, are considered as an important enabler for interoperability and cognitive networking in the underwater domain. Most of the relevant R&D efforts currently taking place, targeting the design of a software-defined modem for the NILUS MK-2 sensor node are also described in [4].

In the proposed work, we are aiming at achieving a 20 kbps link that relies on transmission using multiple transmit front-ends to enable a multiple-input multiple-output system (MIMO). None of the systems available in the market actively employs multiple sound sources for transmissions. The proposed nominal range of the communication link is on the order of a few hundred meters up to 1 km in sea water. A transmitter is being proposed for the deployment of underwater sensor networks and will be deployed in realistic conditions.

In this work, the specific objective is to study the reliability of the MIMO link using a low-complexity modulation technique. Specifically, Frequency Shift Keying (FSK) combined with Multiple - Input Multiple - Output (MIMO) coding is adopted in this work. Non-coherent detection of M-ary Frequency Shift Keying (M-FSK) signals has traditionally been preferred for channels with rapid phase variation, which is particularly difficult to compensate when the channel is relatively shallow [5]. In this work, it is proposed to use multiple elements at the transmitter to improve reliability. Since the channel impulse response is not available at the transmitter, an Alamouti Space Time Block Code (STBC) is adopted. Applying MIMO coding at the transmitter and receiver provides potential spatial diversity gain. In [6], a comparative analysis of various space time codes is provided. To achieve high data rate at high quality of service. Following [6], a particular code has been selected which will provide the best performance with very low complexity. The use of multiple sources reduces the effects of interference and improves diversity gain through coherent combining. Coherent detection is preferable to improve the reliability in comparison to non coherent

detection, however, phase and frequency synchronisation is very challenging in underwater communications. Note that in [7] adaptive equalization is realized to compensate for the channel impairments, and includes a phase locked loop. Hence STBC, which does require channel information at the transmitter with MIMO potentially provides great advantage in increasing the reliability of the communication system. In rich scattering environments, the spectral efficiency and link reliability can be improved in MIMO systems by spatial multiplexing and source gain diversity. Applications of STBC with various modulation techniques has been depicted in literature [8], [9], [10], [7].

1.2 Research Objectives

The goal of this thesis is to quantify the impact of the underwater acoustic channel on the communication system using FSK with MIMO. Realistic measurements at sea will be used to assess how the acoustic channel affects the performance of MIMO systems. As such, the main objectives of this research are: 1) to develop a MIMO SDAM transmitter that can be adapted to varying channel conditions, 2) to assess the performance of a MIMO/FSK system in different deployment scenarios, and 3) study the effects of correlation in MIMO channels in FSK.

1.3 Organization of Thesis

This thesis is organised as follows. In Chapter 2, a model of the MIMO/FSK communication system applied to underwater acoustic propagation is developed, STBC and FSK with non-coherent detection are introduced. In chapter 3, the field work procedure, transmitter design and channel characterisation are presented. In Chapter 4, the methodology applied to extract information from the transmissions recorded during sea trials is explained and results are presented. Chapter 5 elaborates on the findings, makes comparisons between the measured and simulated data, and proposes explanations and conclusions.

Chapter 2

Underwater Acoustic MIMO System

Acoustic propagation is one of the most challenging wireless communication. The absorption increases rapidly with frequency, especially above a few kHz, limiting the usable frequency band to below a few tens of kHz [2]. Underwater acoustic propagation is predominately affected by the sound speed profile of the water column, transmission losses due to signal spreading and absorption, multipath reflections on ocean boundaries, and temporal variations of the ocean due to motion. This chapter explores some of those theories from limited bandwidth due to absorption to Doppler spread, while describing topics such as multipath propagation and Transmission Loss (TL) mechanism and echos.

To support the development of infrastructure along the North American coasts and in the Arctic, underwater sensor networks are proposed to monitor seismic activity, ambient noise, and ecosystem activity. Dense networks spanning 100 square kilometers rely on the deployment of hundreds of low-cost disposable nodes. To maintain network connectivity, it is highly desirable to enable a high speed communication link between nodes and with underwater autonomous vehicles. Here MIMO is proposed to improve the reliability and potentially increase the channel capacity.

Acoustic modems that are reconfigurable at all layers of the communication stack, either by a user or by means of autonomous decisions, are considered as an important enabler for interoperability underwater. The proposed Field Programmable Gate Array (FPGA) based MIMO-SDAM has been demonstrated to provide great flexibility with low maintenance. Because of the increased potential applications for underwater communication, there is a need for high speed transmission. For this purpose, reliable transmission with basic encryption and security is a must, and the proposed platform provides the flexibility to research and develop new space-time coding techniques in realistic settings. A well known MIMO-STBC coding technique was implemented and tested on the proposed platform. Most underwater acoustic modems offer only low data rates. This is largely because they operate at low frequency, which limits the channel bandwidth available, and hence the symbol rate. The low frequency

acoustic channel suffers from substantial multipath and doppler effects, which constrain the signal quality at the receiver. Both commercial and military applications are now calling for real-time communication with submarines and Autonomous Underwater Vehicles (AUVs) in point-to-point as well as in network scenarios. Remote control in the off-shore oil industry, collection of scientific data recorded at ocean-bottom stations and pollution monitoring in environmental systems are name a few.

The objective of this chapter is to provide a high level overview of the background on physical properties of acoustic propagation and system requirements for the proposed communication system. In Section 2.1, the propagation model will be described. The calculations obtained from the model will be used to describe the system requirements. In Section 2.2, the concept of FSK modulation will be introduced. In Section 2.3, a well known STBC technique will be explained and finally in Section 2.4, non-coherent detection of FSK will be described.

2.1 Propagation Model

In this Section, a realistic propagation model to evaluate the communication performance underwater will be described. Specifically, in Section 2.1.1, a link budget will be calculated; then, in Section 2.1.2, the effect of multipath arrival due to boundary reflections, and refraction will be described; in Section 2.1.3, the result of fading due to mobility and variations in the environment as a function of time will be presented. Both these are caused due to relative motion of platforms and the environment.

2.1.1 Link Budget

To achieve the goal of a high speed underwater communication link of up to 1 km, 100 bps, using FSK, with an alternative Phase Shift Keying (PSK) system that can achieve 20 kbps in high SNR conditions, a link budget is calculated for the communication model.

The front end elements shown in Figure 2.1 are three narrowband omnidirectional sound sources with a center frequency close to 27.5 kHz. The signal is amplified to a maximum of $V_{TX} = 10.5$ $\mathrm{V_{RMS}}$ using a linear Power Amplifier (PA) that is directly interfaced to the source. A detailed discussion about the Transmit Voltage Response (TVR) is presented in Section 3.1.

Figure 2.1: Benthowave transducer

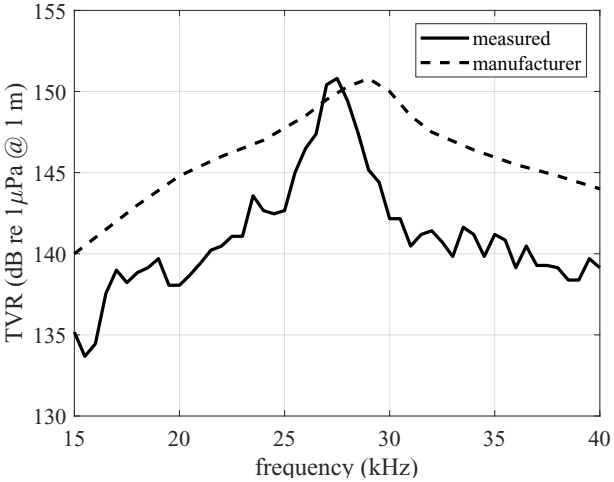

Figure 2.2: Measured transmit voltage response.

The maximum range of the system is estimated using the link budget. For this purpose, the underwater ambient noise Power Spectral Density (PSD) is calculated using Urick's ambient noise model [11]. For low shipping activity, and wind speed on the order of 10 m/sec, the total PSD due to flow noise, shipping activity, surface noise, and thermal noise is estimated to be 67 dBm/Hz. As such, to achieve an signal to noise ratio (SNR) at the receiver equal to 10dB in bandwidth of 5 kHz, the minimum signal intensity level ($\mathrm{SIL_R}$) at the receiver is $\mathrm{SIL_R} = (67 + 10\log(5000) + 10)$ which is equal to $\mathrm{SIL_R} = 113.9$ dBm re 1μPa.

Then, for a transmit power equal to $\mathrm{SIL_T} = 150.2 + 20\log_{10}(10.5)$, which equates to 170.3 dBm re 1μPa, it can found that the maximum transmission loss $\mathrm{TL_M}$ is 56.1 dB. This is obtained for a distance of approximately $10^{\mathrm{TL_M}/20} = 650$ meters. Note that here the effect of absorption at 27.5 kHz is neglected. To increase the distance further, spread spectrum techniques can be applied at the expense of throughput.

2.1.2 Multipath

The concept of multipath arrival and its effect on the underwater communication systems is introduced in this section. A mathematical representation of the multipath communication channel is described.

When a transmitted signal interacts with a boundary, such as the surface or sea floor, a reflection occurs with a departure angle found according to Snell's Law. The departure angle and signal strength of bottom reflections depend upon the consistency and density of the material on the ocean floor. Figure 2.3 shows an example of a 4-path environment including the respective amplitude and distance for each path. The paths consist of an idealized direct path (path 0), a refracted direct path due to change in speed of sound with depth (path 1), a surface reflection (path 2), and a bottom reflection (path 3). These multiple refractions and reflections are delayed versions of the signal and interfere with the original signal. In addition, a varying sound speed profile creates additional bends in the reflected arrivals causing an increasingly complex multipath profile. The discrete channel impulse response (CIR) of a multipath environment is described as the summation of a select number of discrete path arrivals, each arrival with a path dependent amplitude and time delay [12].

Consider a communication channel with multipath. The delay spread of the symbols is τ, and it is a measure of the multipath profile of a underwater communications channel. It is generally defined as the difference between the time of arrival of the earliest component

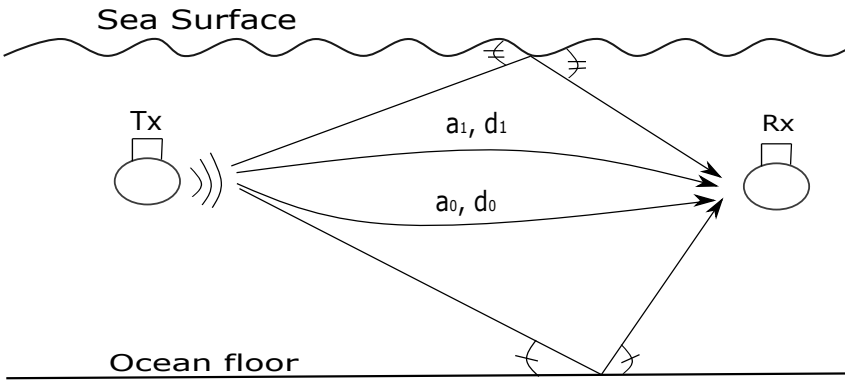

Figure 2.3: Depiction of multipath propagation in sound waves

(e.g., the line-of-sight wave if there exists) and the time of arrival of the latest multipath component. Delay spread is a random variable, and the standard deviation is a common metric to measure it. This measure is widely known as the root-mean-square delay spread σ_τ. The consequence of this delay spread is that the channel bandwidth is limited to certain bandwidth B_c, which is termed as the coherence bandwidth. The coherence bandwidth $B_c = 1/\tau$. It means that for a signal with a bandwidth that is smaller than the channel coherence bandwidth, the signal will suffer only from flat fading. Otherwise, when the bandwidth of the transmitted signal is greater than the coherence channel bandwidth B_c the fading will be frequency selective such that some signal frequencies will be severely attenuated. Such selective fading must be mitigated using frequency domain equalizers. Nonetheless, practical equalizers cannot entirely remove the inter-symbol interference created in a frequency selective channel.

The coherence bandwidth B_c is a statistical measure of the range of frequencies over which the channel can be considered flat (i.e., it passes all spectral components with approximately equal gain and linear phase). All frequency components of the transmitted signal within the coherence bandwidth will fade simultaneously. The coherence bandwidth is inversely proportional to the delay spread, and we thus have the following:

$$B_c = 1/\sigma_\tau$$

The delay spread σ_τ and the coherent bandwidth B_c are parameters that describe the

time dispersion nature of the underwater channel and their values with respect to the transmitted signal bandwidth B_s and the symbol duration T_s can help determine if the channel is experiencing flat fading or frequency-selective fading.

The difference between path lengths is rarely greater than a few meters, so the delay spread σ_τ is rarely more than several milliseconds. The coherence bandwidth B_c is thus typically greater than 10 Hz [13]. If a channel is faded at one frequency, the signal may be transmitted at a different frequency, that is separated by the original frequency by at least B_c.

In underwater communications, when echo spans more than the symbol time there will be inter-symbol interference(ISI). In contrast, when the path arrivals within one symbol time period, the paths combine non-coherently, and as such the channel may be subject to significant amplitude variations. This is fading. MIMO can mitigate the effect of fading, and can actually uses the diversity to enhance the system capacity. Specifically, a MIMO system utilizes uncorrelated fading channels to create communication links that are orthogonal to each other. As such, in an $M \times N$ MIMO system, as many as $\min(M, N)$ in parallel communication channels can be created.

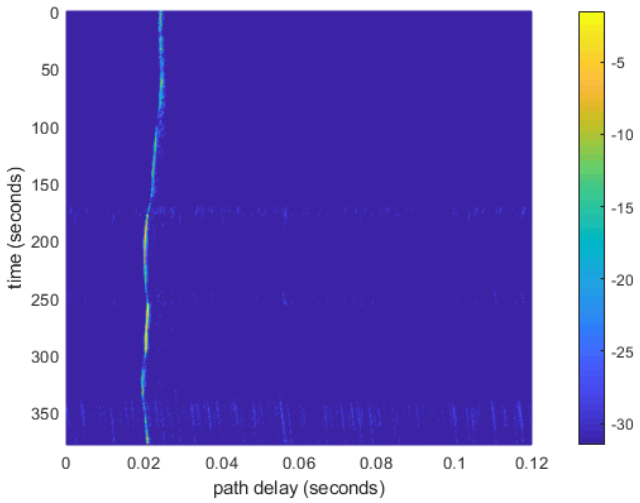

Figure 2.4: Channel impulse response at 200m in Halifax's North West Arm

In this work, during various measurement campaigns, a pseudo-random noise (PRN) sequence was used to assess the channel characteristics. An example of the time-varying channel impulse response as a function of time taken in the Halifax North West Arm is shown in Fig. 2.4 and is representative of the propagation conditions in that area. By post-processing of the data, channel statistics, such as the transmission loss, the doppler

spread and delay spread were obtained. These results will be presented in Section 3.3. More importantly, that the spatial correlation is computed and it is demonstrated that it remains relatively high, even for separations between the elements that are greater than 10 λ. Next section describes the effect of mobility in the channel.

2.1.3 Fading

The Doppler spread B_d is a measure of spectral broadening caused by the rate of change of the underwater communication channel and is defined as the range of frequencies over which the received Doppler spectrum is essentially nonzero. When the bandwidth of the transmitted signal is much larger than the Doppler spread, the effects of the Doppler spread are negligible at the receiver. The coherence time T_c is a statistical measure of the time duration over which the channel impulse response essentially remains unchanged (i.e., highly correlated). If the time interval between the signal transmissions is much greater than the coherence time, the channel will likely affect the two signal transmissions differently; otherwise, they will be affected similarly. The Doppler spread is inversely proportional to the coherence time, and we thus have:

$$B_d = 1/T_c$$

Doppler spread and coherence time are parameters that describe the frequency-dispersion nature of the underwater communication channel, and their values with respect to the transmitted signal bandwidth B_s and the symbol duration period T_s can help determine if the channel is experiencing fast fading or slow fading. The coherence time T_c is fundamentally interpreted as the order-of-magnitude duration of a fade at a given frequency. The Doppler shift and Doppler spread are both linear functions of the signal frequency. The variation of Doppler spread with frequency is important when the operating frequency bands are different. For instance, a system operating at 20 kHz has a Doppler spread twice that of a 10 kHz system, and thus resulting in a coherence time half as large. This gives rise to faster fading, with shorter fade duration, and channel measurements that become outdated twice as fast.

2.2 Frequency Shift Keying

In this work, FSK is adopted to create a reliable communication link. In Section 2.2.1, Minimum Shift Keying (MSK) will be considered as a spectral efficient modulation technique, while in Section 2.2.2, a more general Continuous Phase Frequency Shift keying (CPFSK) modulation technique is adopted.

2.2.1 Minimum Shift Keying

As part of this work, an MSK communication system model was modelled using MATLAB in comparison to Orthogonal frequency-division multiplexing (OFDM), or Quadrature amplitude modulation (QAM). It was considered because it offers advantages in terms of spectral efficiency when compared to other similar modulations. As depicted in Figure 2.5, not only does it have a constant envelope, but it also has a continuous phase. Also, the bandwidth requirements for MSK are half as much as those for Binary- FSK (BFSK) and Binary-PSK (BPSK), respectively, while their bit error rates are no greater than their other binary counterparts.

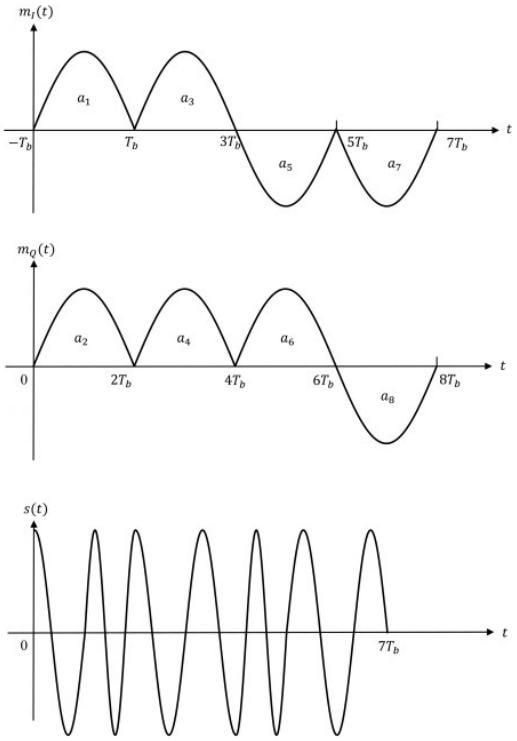

Figure 2.5: MSK modulation

The binary data consisting of sharp transitions between "one" and "zero" states and vice versa potentially creates signals that have sidebands extending out a long way from the carrier, and this creates problems for many communications systems, as any sidebands outside the allowed bandwidth cause interference to adjacent channels and any other communications links that may be using them. MSK, has no phase discontinuities and this significantly reduces the bandwidth needed over other forms of phase and frequency shift keying. The frequency changes occur at the carrier zero crossing points. The modulating data signal changes the frequency of the signal. This arises as a result of the unique factor of MSK that the frequency difference between the logical one and logical zero states is always equal to half the data rate. This can be expressed in terms of the modulation index (h), and it is always equal to 0.5.

Due to the constraint that the frequency difference between the logical one and logical zero states is always equal to half the data rate for MSK, other modulation schemes were explored. In particular CPFSK introduces in the next section was studied extensively.

2.2.2 Continuous Phase Frequency Shift Keying

In this section, the CPFSK modulation scheme is introduced. A analytical baseband model using continuous phase shift keying representation is derived and is augmented with the STBC later in Section 2.3.2.

The implementation of CPFSK removes the phase discontinuities present in an FSK system. Also, on FPGA, the direct digital synthesizer (DDS) implements a signal that has continuous phase. The change in the phase from the DDS translates to change in the frequency. Hence, a CPFSK waveform is produced as a result. For this purpose, CPFSK was implemented at the transmitter in this work.

CPFSK can be considered as a general form of MSK with varying value of the modulation index. Variations in the modulation index results in change in the modulation scheme. In the following paragraphs, a mathematical representation of the baseband CPFSK is derived.

In conventional FSK modulation, the signal is generated by shifting the carrier by an amount $m\Delta f, 1 \leq m \leq M$, to reflect the digital information that is being transmitted. As explained in [14], to avoid the use of signals having large spectral side lobes, the information-bearing signal frequency modulates a single carrier whose frequency is changed continuously. The resulting frequency modulated signal is phase-continuous, and hence, it is called

continuous-phase FSK.

A mathematical representation of the CPFSK is presented in the following few paragraphs. A Pulse amplitude modulation (PAM) signal is represented as

$$d(t) = \sum_n I_n g(t - nT) \tag{2.1}$$

where I_n denotes the sequence of amplitudes obtained by mapping A:-bit blocks of binary digits from the information sequence a_n into the amplitude levels $\pm 1, \pm 3, \cdots, \pm(M-1)$ and $g(t)$ is a rectangular pulse of amplitude $1/2T$ and duration T seconds. The signal $d(t)$ is used to frequency-modulate the carrier. Consequently, the equivalent lowpass waveform $v(t)$ is expressed as

$$v(t) = \sqrt{\frac{2E}{T}} e^{j[4\pi T f_d \int_{-\infty}^{t} d(\tau)d\tau + \phi_0]} \tag{2.2}$$

where f_d is the *peak frequency deviation* and ϕ_0 is the initial phase of the carrier. The carrier-modulated signal corresponding to Equation 2.2 may be expressed as

$$c(t) = \sqrt{\frac{2E}{T}} cos[2\pi f_c t + \phi(t; \boldsymbol{I}) + \phi_0] \tag{2.3}$$

where $\phi(t; \boldsymbol{I})$ represents the time-varying phase of the carrier, which is defined as

$$\phi(t; \boldsymbol{I}) = 4\pi T f_d \int_{-\infty}^{t} d(\tau)d\tau$$

$$= 4\pi T f_d \int_{-\infty}^{t} \left[\sum_n I_n g(\tau - nT)] \right] d\tau \tag{2.4}$$

Note that, although $d(\tau)$ contains discontinuities, the integral of $d(\tau)$ is continuous. Hence, we have a continuous-phase signal. The phase of the carrier in the interval $nT \leq t \leq (n+1)T$ is determined by integrating 2.4. Thus,

$$\phi(t; \boldsymbol{I}) = 2\pi f_d T \sum_{k=-\infty}^{n-1} I_k + 2\pi f_d q(t - nT) I_n$$

$$= \theta_n + 2\pi f_d q(t - nT) I_n \tag{2.5}$$

where h, θ_n and $q(t)$ are defined as

$$h = 2f_d T$$

$$\theta_n = \pi h \sum_{k=-\infty}^{n-1} I_k$$

$$q(t) = \left\{ \begin{array}{cc} 0 & \text{t } <0 \\ \dfrac{t}{2T} & 0 \leq t \leq T \\ \dfrac{1}{2} & \text{t } > \text{T} \end{array} \right\}$$

The θ_n represents the accumulation (memory) of all symbols up to time $(n-1)T$. The parameter h is called the *modulation index*.

Using CPFSK, the phase $\phi(t; \boldsymbol{I})$ of the carrier can be expressed as [14]:

$$\phi(t; \boldsymbol{I}) = 2\pi \sum_{k=-\infty}^{n} I_k h_k q(t - kT), \qquad nT \leq t \leq (n+1)T \tag{2.6}$$

where I_k is the sequence of M-ary information symbols selected from the alphabets $\pm 1, \pm 3, \cdot\cdot\cdot, \pm(M-1)$ and where h_k is a sequence of modulation indices, and $q(t)$ is some normalized waveform shape, with symbol duration T. Then, the output of the modulator is a baseband representation of the modulated signal given by:

$$s(t) = \exp\left[j2\pi \sum_{k=0}^{n} I_k h_k q(t - kT) \right], \qquad nT \leq t \leq (n+1)T \tag{2.7}$$

The continuous waveform signal derived in 2.7, then coded with STBC to generate a MIMO-FSK modulation technique for the transmission.

2.3 Space Time Block Coding

MIMO underwater architectures have been studied for several years now, but the technology was historically reserved for Radio Frequency(RF) systems. In section 2.3.1, theoretical aspect of MIMO is introduced, along with review of the top three reasons why, despite added complexity and costs, MIMO communications are beneficial for underwater communications. Then in a first instance, in Section 2.3.2 analytical baseband model of CPFSK will be augmented with STBC.

2.3.1 MIMO Background Theory

This section introduces the background theory on MIMO and top three reason why underwater MIMO communications should be beneficial.

MIMO systems increase the number of transmit and received signals from one to four or more. Thus, in order to deliver MIMO functionality, an underwater transceiver must be able to control multiple sources and hydrophones. The technique requires complex processing and switching that provides control over each sound source. As expected, the added complexity increases cost and design time. By enabling spatial channelization and diversity, MIMO expands the bandwidth available within a given spectral bandwidth and space. There are three MIMO transmission techniques, and each offers an opportunity to selectively and adaptively optimize the space and bandwidth already in use.

Beam steering – MIMO offers the opportunity to electronically guide the directivity of the sound signal by controlling the signal propagating phase over multiple antennas. This provides two major benefits: first, beam steering can directionally focus the sound energy on a single user, ignoring the remaining space. It is also possible to track the user, reducing interference and boosting signal to noise wherever the user is located. Secondly, beam steering can solve the problem of multipath by discovering the best path and targeting energy toward that direction. Even when transceivers are stationary, environmental changes affect the many paths that a signal can take, so dynamically adjusting and selecting the best path maintains best connectivity and increases range in high interference environments.

Increased data capacity – MIMO can add data carrying capacity without requiring additional bandwidth through spatial multiplexing. The long-established Shannon-Hartley theorem states that the data carrying capacity(C) of a channel is proportional to its bandwidth (B) in Hertz:

$$C = B \log_2(1 + S/N). \tag{2.8}$$

MIMO offers the advantage of channelizing the space: each spatial channel can become independent, thus breaking through the limits posed by Shannon-Hartley. Following few paragraphs summarize the method of a transformation to convert a matrix channel into a set of parallel independent sub-channels explained in [15].

Consider a narrowband time-invariant underwater communications channel with n_t transmit and n_r receive antennas is described by an n_r by n_t deterministic channel matrix $\mathbf{H}$.

Singular value decomposition of $\mathbf{H}$ determines spatial multiplexing and capacity. The time-invariant channel is described by

$$\mathbf{y} = \mathbf{H}\mathbf{x} + \mathbf{w}, \tag{2.9}$$

where $\mathbf{x} \in \zeta^{n_t}$ $\mathbf{y} \in \zeta^{n_r}$ and $\mathbf{w} \sim \zeta(0,N_o\mathbf{I}_{n_r})$ denote the transmitted signal, received signal and white Gaussian noise respectively at a symbol time (the time index is dropped for simplicity). The channel matrix $\mathbf{H} \in \zeta^{n_r \times n_t}$ is deterministic and assumed to be constant at all times and known to both the transmitter and the receiver. Here, h_{ij} is the channel gain from transmit antenna j to receive antenna i. There is a total power constraint, P, on the signals from the transmit antennas. At the receiver, the signal is also subject to AWGN. The capacity can be computed by decomposing the vector channel into a set of parallel, independent scalar Gaussian sub-channels. From basic linear algebra, every linear transformation can be represented as a composition of three operations: a rotation operation, a scaling operation, and another rotation operation. In the notation of matrices, the matrix $\mathbf{H}$ has a *singular value decomposition* (SVD):

$$\mathbf{H} = \cup\wedge\vee^* \tag{2.10}$$

where $\cup \in \zeta^{n_r \times n_r}$ and $\vee \in \zeta^{n_t \times n_t}$ are (rotation) unitary matrices and $\wedge \in \mathbb{R}^{n_r \times n_r}$ is a rectangular matrix whose diagonal elements are non-negative real numbers and whose off-diagonal elements are zero. The diagonal elements $\lambda_1 \geq \lambda_2 \geq \cdots \lambda_{n_min}$ are the ordered *singular values* of the matrix $\mathbf{H}$, where $n_{min} = \min(n_t, n_r)$. Since,

$$\mathbf{H}\mathbf{H}^* = \cup\wedge\wedge^t\cup^*, \tag{2.11}$$

the squared singular values λ_i^2 are the eigenvalues of the matrix $\mathbf{H}\mathbf{H}^*$ and also of $\mathbf{H}^*\mathbf{H}$. Note that there are n_{min} singular values. We can rewrite the SVD as

$$\mathbf{H} = \sum_{i=1}^{n_{min}} \lambda_i u_i v_i^*, \tag{2.12}$$

i.e., the sum of rank-one matrices $\lambda_i u_i v_i^*$. It can be seen that the rank of $\mathbf{H}$ is precisely the number of non-zero singular values. If we define

$$\tilde{\mathbf{x}} = \vee^*\mathbf{x}, \tag{2.13}$$

$$\tilde{\mathbf{y}} = \cup^* \mathbf{y}, \tag{2.14}$$

$$\tilde{\mathbf{w}} = \cup^* \mathbf{w}, \tag{2.15}$$

then we can rewrite the channel (Equation: 2.9) as

$$\tilde{\mathbf{y}} = \wedge \tilde{\mathbf{x}} + \tilde{\mathbf{w}}, \tag{2.16}$$

where $\tilde{\mathbf{w}} \sim \zeta(0, N_o \mathbf{I}_{n_r})$ has the same distribution as $\mathbf{w}$ and $\| \tilde{\mathbf{x}} \|^2 = \| \mathbf{x} \|^2$. Thus, the energy is preserved and we have an equivalent representation as a parallel Gaussian channel:

$$\tilde{y}_i = \lambda_i \tilde{x}_i + \tilde{w}_i, \qquad i = 1, 2, \ldots, n_{min} \tag{2.17}$$

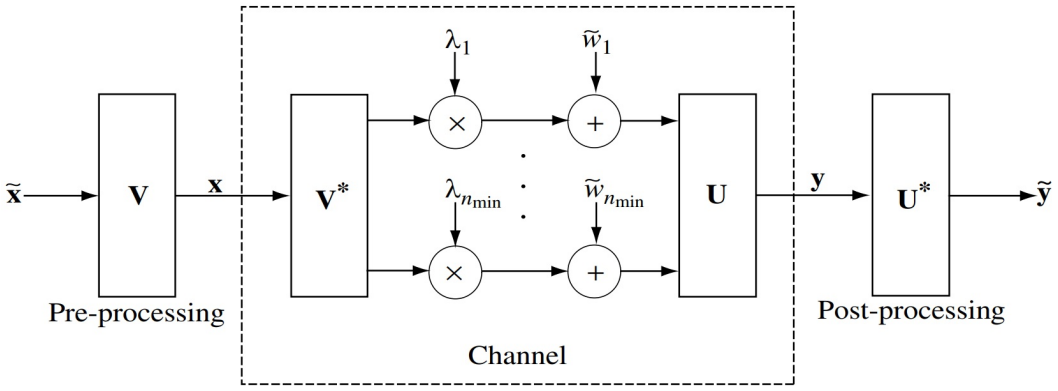

Figure 2.6: Converting MIMO channels into a parallel channel through the SVD

The equivalence is summarized in Figure 2.6. The SVD decomposition can be interpreted as two *coordinate transformations*: it says that if the input is expressed in terms of a coordinate system defined by the columns of $\vee$ and the output is expressed in terms of a coordinate system defined by the columns of $\cup$, then the input/output relationship is very simple. Equation 2.16 is a representation of the original channel (Equation: 2.9) with the input and output expressed in terms of these new coordinates. Here, the spatial dimension plays the same role as the time and frequency dimensions in improving capacity. The capacity given by

$$C = \sum_{i=1}^{n_{min}} \log \left(1 + \frac{P_i^* \lambda_i^2}{N_o} \right) \quad \text{bits/s/Hz}, \tag{2.18}$$

where $P_1^*,\cdots,P_{n_{min}}^*$ are the waterfilling power allocations:

$$P_i^* = (\mu - \frac{N_o}{\lambda_i^2}) \tag{2.19}$$

with μ chosen to satisfy the total power constrain $\sum_i P_i^* = P$. Each λ_i corresponds to an *eigenmode* of the channel (also called an *eigenchannel*). Each non-zero eigenchannel can support a data stream; thus, the MIMO channel can support the spatial multiplexing of multiple streams. Figure 2.7 pictorially depicts the SVD-based architecture for reliable communication.

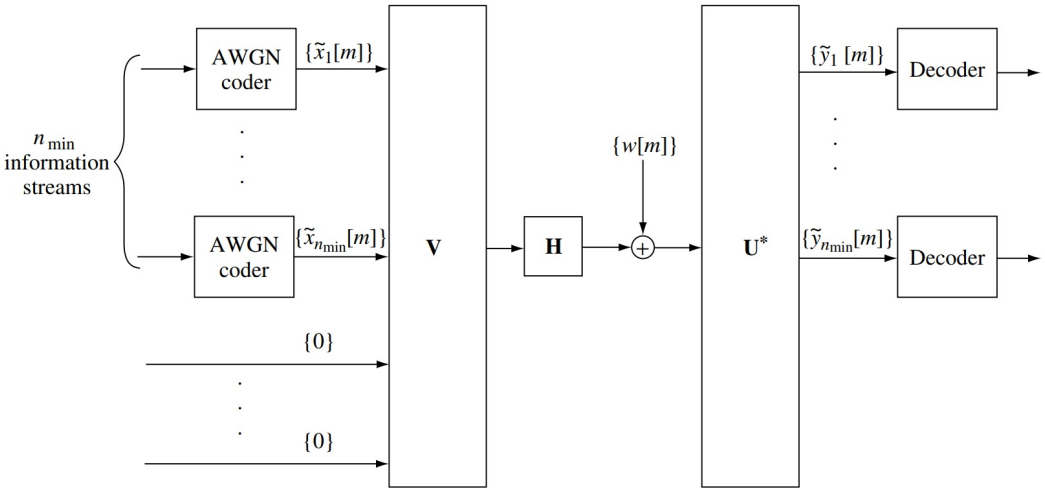

Figure 2.7: The SVD architecture for MIMO communications

Although an arbitrary number of spatial channels is not practical, the ability to increase data rate by 50 %, or perhaps double, within the same bandwidth use is a major advantage.

Diversity – As MIMO offers the ability to distinguish transmission over multiple paths, it is possible to encode the signal more efficiently if the effect of those paths is considered. Space-time encoding uses optimally encoded versions of the transmission, knowing that each version will be received with varying delays and signal-to-noise ratios. The encoding aims to compensate for losses and added noise through each of the spatial channels within a MIMO transmission while also adding redundancy that can correct bit errors. This type of encoding requires the use of multiple channels, each with independent delay and loss. Thus, a single antenna system cannot make use of this technique.

All three MIMO transmission techniques improve performance beyond the capability of a

single antenna system: controlling the path and focusing on tight spaces through beam steering allows high density underwater deployments. Spatial multiplexing allow increased data transmission through a constrained bandwidth space if the channels can maintain similar signal-to-noise ratios. Diversity is ideal for ensuring important data is not lost when transferring through a noisy channel, especially when bandwidth is not as constrained. Collectively, these MIMO techniques enable improved signal range, reduced bit errors, lower power consumption, reduced interference and even enhanced non-line-of-sight (NLOS) or quasi-NLOS connectivity. Thus, the advantages provided quickly outnumber any disadvantages related to initial cost or design complexity. MIMO systems are successful with applications requiring high data rate, high Quality of Service (QoS) and increased range.

2.3.2 Alamouti/FSK

In this section, the benefit of an Alamouti STBC code using (M-CPFSK) will be demonstrated analytically. In this section CPFSK will be augmented with the STBC.

The Alamouti scheme improves the signal quality at the receiver by simple processing across two transmit sound sources. Hence, it reduces the processing at the receiver exponentially as a function of bandwidth efficiency (bits/s/Hz).

In this work, the Alamouti STBC is chosen to implement spatial diversity at the transmitter. The Alamouti code does not require channel state information (CSI) at the transmitter. While the performance of the Alamouti STBC is tested for a 2x1 MISO scenario, it can be generalized to two transmit antennas and M receive antennas to provide a diversity order of 2M. The Alamouti scheme is developed in [16]. In this technique symbols are repeated over certain number of transmit antennas. Other techniques such as, delay diversity for base station simulcasting [17] [18], the creation of an artificial multipath distortion using copies of same signal at different time by Seshadri and Winters together and independently [19] [20] were also investigated.

Figure 2.8 shows the baseband representation of two transmitter sources and one receive hydrophone. At the transmitter the data frame is encoded, while at the receiver it is decoded to maximize reliability, and equalized to compensate for multipath distortion.

The Alamouti scheme may be defined by the following three functions. Namely, encoding and transmission of the information sequence, combining sequence at the receiver and equalization and decision making.

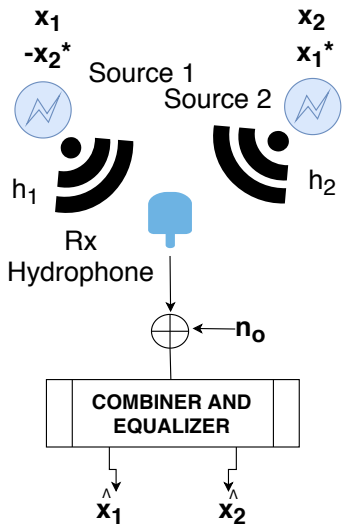

Figure 2.8: MIMO STBC system model

Let x_1 and x_2 be the modulated transmit symbols prior to the STBC encoder to be transmitted from Source #1 and Source #2 respectively. At the output of the STBC encoder, the signals are encoded on two consecutive time slots of duration T. In the first time slot t, they are unchanged, while during the next symbol period $-x_2^*$ is transmitted from Source #1, and x_1^* is transmitted from Source #2. This is summarized in Table 2.1.

Assuming a frequency flat channel, the channel amplitude from Source #1 and Source #2 are h_1 and h_2 respectively. Note that the channels are constant with time t and $t+T$, where T is the code duration duration. The received signals y_1 at time t and y_2 at time $t+T$ can then be expressed respectively as

$$y_1 = h_1 x_1 + h_2 x_2 + n_1,$$

$$y_2 = -h_1 x_2^* + h_2 x_1^* + n_2,$$

where n_1 and n_2 are complex random variables representing the receiver noise and interference.

	Source 1	Source 2
time t	x_1	x_2
time t + T	$-x_2^*$	x_1^*

Table 2.1: Alamouti STBC - Two branch transmit diversity scheme

As shown in Figure 2.8, the two signals at the receiver can be combined as:

$$\hat{x}_1 = h_1^* y_1 + h_2 y_2^* + n_1,$$

$$\hat{x}_2 = h_2^* y_1 - h_1 y_2^* + n_2,$$

where $\hat{x}_1$ and $\hat{x}_2$ are estimates of x_1 and x_2. To recover the binary information, the sequence $\hat{x}_1$ of $\hat{x}_2$ is applied to the CPFSK demodulator.

In a multipath environment, the Alamouti decoder implementation can be enhanced with an equalizer, and in this work two recursive least square equalizers are implemented: the first minimizes the error between $\hat{x}_1$ and the transmit signal x_1, and the second minimizes the error between $\hat{x}_2$ and the transmit signal x_2, as suggested in [21].

2.4 Non-coherent Detection of Frequency Shift Keying

This section discusses the properties of non-coherent modulation techniques proposed for underwater communication. For each of the proposed algorithms, the concept of orthogonality and phase coherence will be discussed. Discussion about the detection of signal in the absence of channel information at the transmitter using STBC follows.

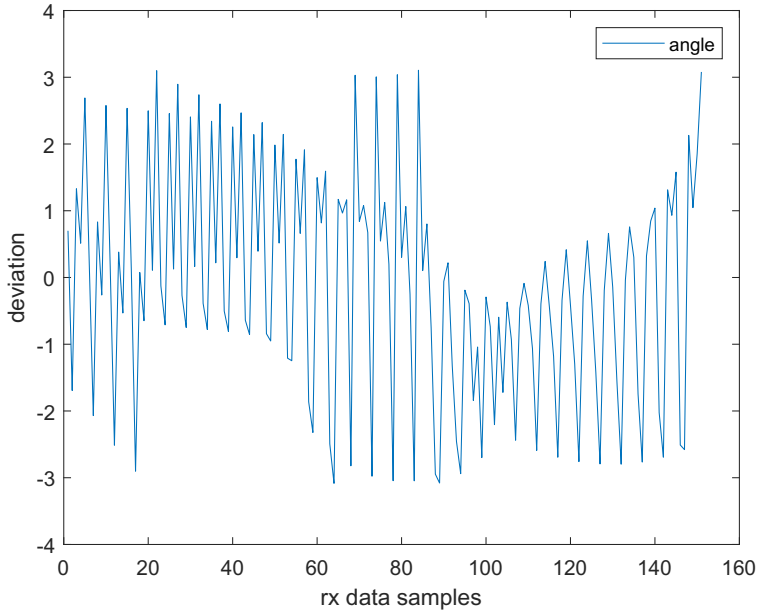

Figure 2.9: Ambiguities in the phase of received data

As a part of this work coherent detection was attempted due to its better performance. Coherency implies that the phase of each mark or space tone has a fixed phase relationship

with respect to a reference. It is complicated to process the data coherently because of synchronisation issue, theoretically, it provides a better reliability than the non-coherent receiver. Figure 2.9, shows the phase of the signal at the input to the decoder. Upon detection and during the processing of data, it was found that the phase of the signal was variable. Ideally, the phase would need to be constant. Although, a phase locked loop (PLL) would be required to avoid variation of phase, the variation in channel as a function of time makes the phase of the data vary very quickly, and it would be very difficult to implement a PLL that can track the phase variation. Instead, non-coherent detection methods are used in this work. Non-coherent detection do not require a PLL, which reduces the complexity of the receiver. It is worth mention here that PLL does increase the performance of the system.

In FSK, different frequencies are used to signal different messages. In comparison to OFDM, FSK sends one frequency at a time. The receiver listens to a set of frequencies and determines which frequency has the largest signal. This frequency represents a specific bit combination. A 1-bit FSK spectrum PSD is illustrated in Figure 2.10. Binary data is converted to a continuous waveform with center frequency of $f_c = 27.5KHz$.

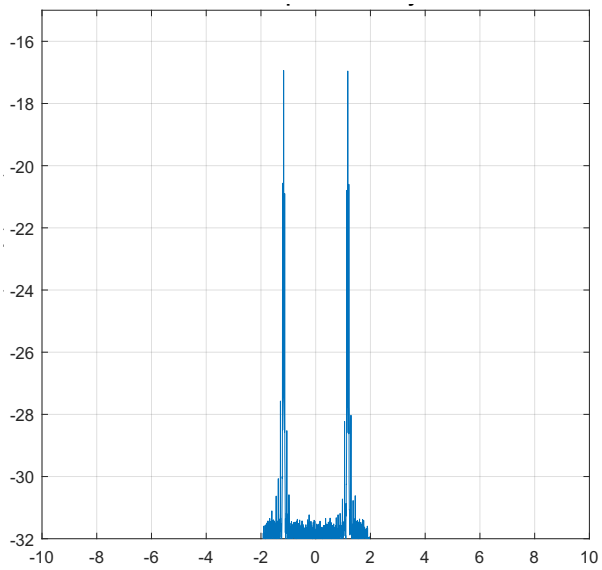

Figure 2.10: FSK baseband frequency response PSD

There are mainly two methods to detect the FSK signal at the receive. Coherent and non coherent detection. Coherency is similar to generating an FSK signal by switching between two fixed-frequency oscillators to produce the mark and space frequencies. While this method is sometimes used, the constraint that transitions from mark to space and vice

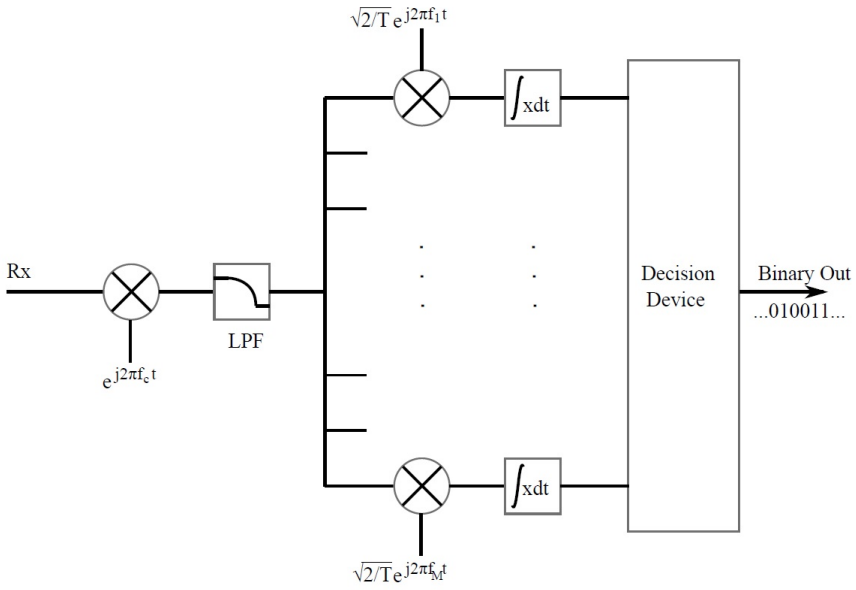

Figure 2.11: Non-coherent M-FSK receiver

versa must be phase continuous ("glitch" free) requires that the shift and keying rate be interrelated. A synchronous FSK signal which has a shift in Hertz equal to an exact integral multiple (n = 1, 2,...) of the keying rate in bauds, is the most common form of coherent FSK. Coherent FSK is capable of superior error performance but noncoherent FSK is simpler to generate and is used for the majority of FSK transmissions. Noncoherent FSK has no special phase relationship between consecutive elements, and, in general, the phase varies randomly.

Alternatively, simple non-coherent receivers are easily implemented because the phase information is not required; but this sacrifices reliability. Non-coherent receivers typically employ energy detection for each subcarrier. A simple structure may be represented by down-converting, or bandshifting, using a common center frequency, low pass filtering, and parallel energy detection of subcarriers, shown in Figure 2.11. Energy detection is accomplished by further downconverting the received signal, by each subcarrier frequency, integration of the downconverted signal, and sampling before entering the decision device. This type of receiver is known as a correlation receiver.

A similar receiver structure was implemented and used for data processing.

Chapter 3

Implementation and Experimentation

Two Sea trials were performed to test the communications system in very different communications channel conditions. Also, two different receiver array configurations were used. This chapter explains the methodology of implementation and experimentation.

A sea trial was performed in the North West Arm (NWA), Halifax, Nova Scotia on July 31st 2019 to test STBC MIMO underwater communication algorithms. Another sea trial was performed at Grand Passage in the Bay of Fundy.

The objective was to demonstrate the communication performance in controlled underwater acoustic environmental conditions. Prior to the sea trial, several tests were run on land and at sea to calibrate the hardware. The objective of these calibration tests was to demonstrate the performance of key physical-layer sub-systems in realistic underwater deployments. In Section 3.1, the hardware of the system is described for the transmitter and receiver. Section 3.2, describes the procedure and deployment and finally Section 3.3 discusses the channel characterizations procedure and results.

3.1 Transmitter Design

In this section the transmitter design and parameters are presented. FPGA architecture with front end and filter designs are also discussed.

The modem is built using general-purpose (GP) computing architectures running open-source operating system and tools, thereby making a further step toward software-defined open-architecture underwater acoustic modems. The first field tests of the Modem node in multihop underwater acoustic networks are presented, showing satisfactory performance in shallow, noisy and open waters.

The reconfigurable digital platform will be described. The underwater acoustic transmitter firmware is implemented on an Artix-7 FPGA from Xilinx. The transmitter performs encoding, modulation, and up-conversion of the binary source. The transmitter symbol rate R_s is fixed at 5 kBd to meet the bandwidth constraints of the piezoelectric sound source as

specified by the manufacturer. The effective bit rate is equal to $R_b = R_s \log_2(M) R_c$, where M is the modulation index, and $R_c = k/n$ is the code rate.

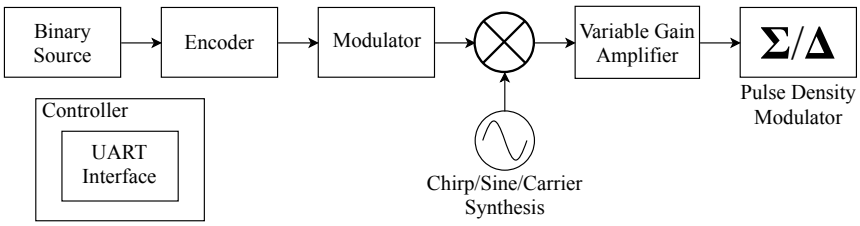

Figure 3.1: High level FPGA firmware architecture

Various parameters of the SDAM saved in the FPGA control unit can be configured through the datapath. Specifically, a digital amplifier controls the amplitude of the signal produced by the digital processor, and the gain of the amplifier can be reconfigured by the user. The control unit can be configured to transmit different sequences of waveforms, that are optionally separated by guard intervals. To upconvert the signal, a sinusoid signal is generated using a direct digitized filter (DDS) that is configured using a phase increment, which defines the signal frequency.

To allow transmission from multiple elements simultaneously, the payload transmitted is encoded using a 1023-symbol long PRN with good auto-correlation properties. The 5-kBd modulated data is filtered using a cascade of a raised cosine filter as well as an interpolation filter that is sampled at 10 MHz, and the coefficients are defined to provide an excess bandwidth of 0.5. Before the signal is applied to the PDM, it is upconverted using a direct sequence synthesizer with a user-reconfigurable frequency. The FPGA processor is programmed to produce three independent modulated streams of information and that are multiplexed on each transducer.

In Fig. 3.2, a block diagram of the M-QAM modulator is shown. Usig M-QAM modulation, the binary sequence is encoded using (M) bits and for a fixed symbol rate R_s, the binary sequence clock rate is $R_b = R_s \log_2(M)$. The output of the modulator is de-multiplexed to represent the in-phase and quadrature values.

Similarly, a 20 kHz PN sequence generator, which is converted to two parallel streams is used to generate the QPSK even and odd data streams. The generator polynomial of $p(z) = z^{12} + z^{11} + z^8 + z^6 + 1$ is used which produces the 4095 bit sequence. This sequence is used to produce the 10KHz and 20Khz PN sequence.

The root raised cosine (RRC) filter pulse shapes the data stream input to limit the signal

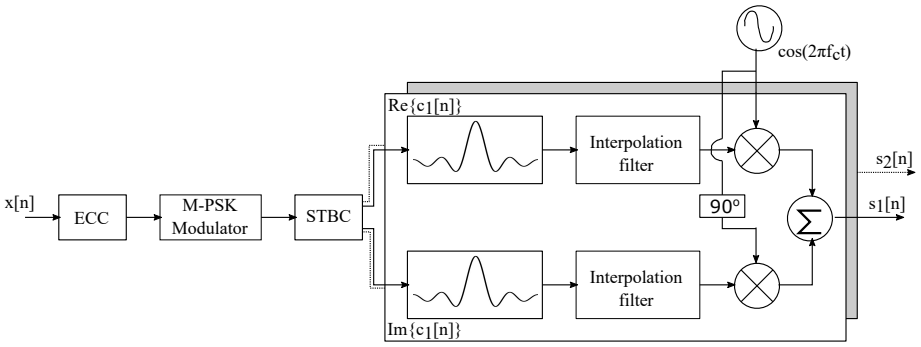

Figure 3.2: M-PSK transmitter block diagram

bandwidth. The interpolation filter up-samples the RRC filter output, such that its sampling frequency matches the sampling frequency of the PDM.

The RRC filter is implemented using an 801th order finite impulse response (FIR) filter. Coefficients were generated in Matlab with a damping factor of 0.5 and a total span of 10 symbols. The input data stream is oversampled by a factor of 80, which requires a clocking frequency of 800 kHz. The interpolation filter is implemented using an 251th order FIR filter. The input data stream is oversampled by a factor of 25, which requires a clocking frequency of 20 MHz. The interpolation filter coefficients are quantized to a word length of 22. This provides enough resolution to accurately produce the expected filter response.

To implement M-CPFSK, instead of implementing a modulator at baseband, in this program, the frequency of the DDS is controlled depending on the symbol to be transmitted. Since the DDS compiler is input a phase increment, this methodology ensures that continuous phase is respected.

The phase input to the DDS is equal to:

$$\theta_i = \frac{f_i 2^{28}}{100 \times 10^6}, \text{ where } i = 1, 2.$$

Here, f_1 and f_2 are defined by the user through the user interface.

Also, as an alternative modulation technique, the LFM has received recent interest to implement reliable underwater acoustic communication links (citations). As such, the DDS compiler is also configured to generate an LFM that sweeps over the symbol time T_{LFM} from a minimum frequency f_{min} to a maximum frequency f_{max}. The instantaneous frequency is fixed by continuously updating the phase at the sample rate.

As such, the minimum frequency f_{min} and maximum frequency f_{max} are defined using

the phases:

$$\theta_{min} = \frac{f_{min}2^{28}}{100 \times 10^6} \quad \text{and} \quad \theta_{max} = \frac{f_{max}2^{28}}{100 \times 10^6}$$

while the phase increment is defined by the phase:

$$\theta_{inc} = \frac{(\theta_{max} - \theta_{min}) \times 10^9}{100 \times 10^6 T_{LFM}}$$

where the symbol period T_{LFM} is in μsec.

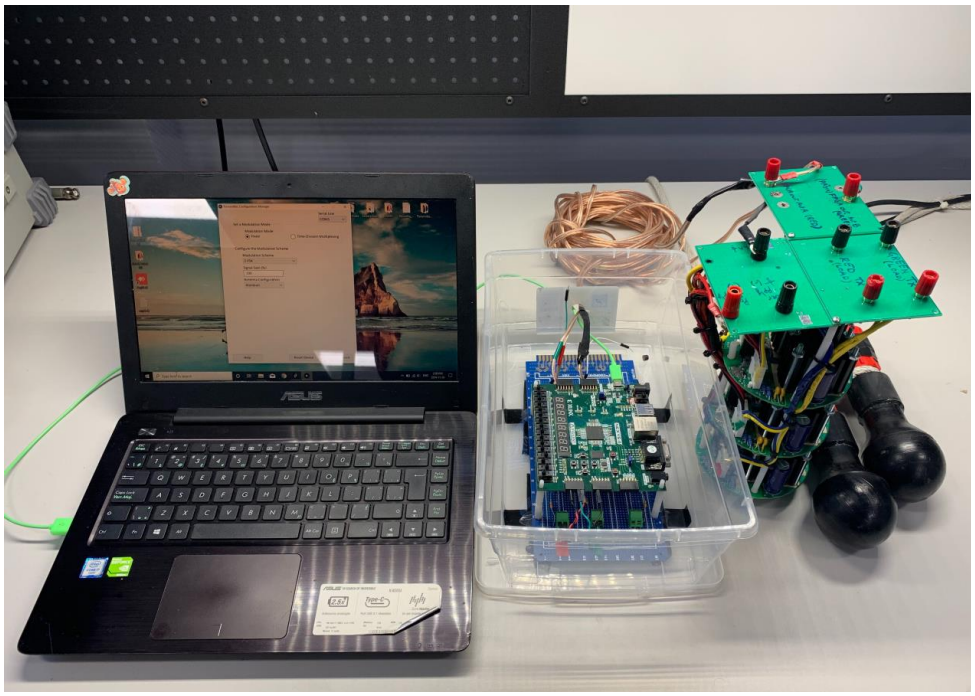

Figure 3.3: Hardware front end

To convert the digital signal to analog, as shown in Figure 3.4 a second order sigma/delta digital-to-analog converter (DAC) that produces a pulse density modulation output (PDM) is implemented on the fabric. The output of the PDM is applied to an analog 3rd order low-pass filter to recover the envelope of the signal as shown in Figure 3.5. The filter is implemented using discrete components as shown in Figure 3.3. It has a 3rd order low-pass Butterworth filter and is designed to have a 3-dB cutoff frequency of approximately 85 kHz. The passive filter design procedure is documented in [22]. The 330-Omega resistor represents the FPGA output resistance, and a ratio of R_{load}/R_{source} is chosen to mitigate the

voltage drop between the input and output of the filter. The output of the filter is applied to a pre-amplifier before it is fed to the power amplifier. In this work, the DAC clocking frequency is 10 MHz. The maximum signal to noise ratio (SNR) of the DAC output signal is approximately 58 dB, and as such represents a signal with an effective number of bits (ENOB) between 8 and 9 for signals below 85 kHz.

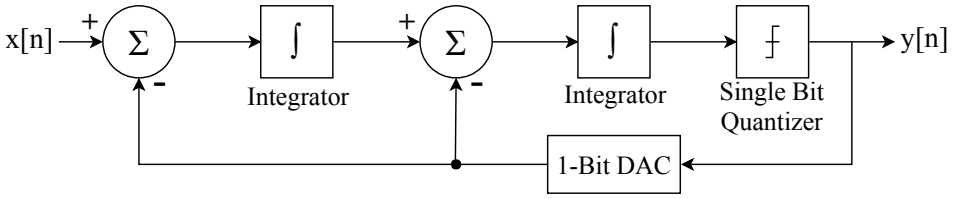

Figure 3.4: Sigma delta modulator block diagram

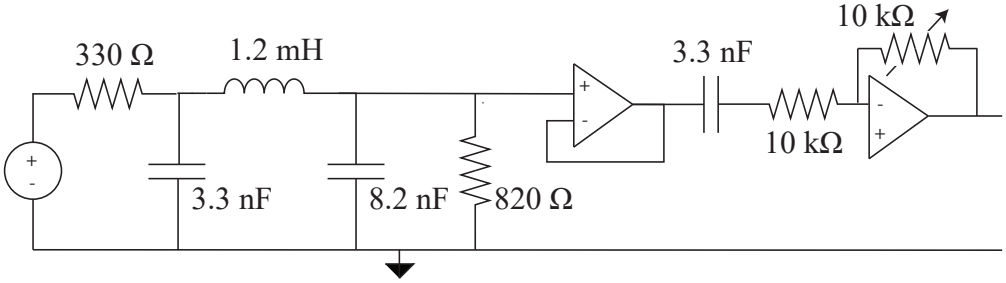

Figure 3.5: Analog filter implementation

The transmitter shown in Figure 3.3 consists of three narrowband omnidirectional sound sources with a center frequency close to 28 kHz. The signal is amplified to a maximum of $V_{TX} = 25.4$ V_{RMS} using a linear power amplifier (PA) that is directly interfaced to the source. A 5-meter cable serves to deploy the sources from a pier or vessel, while keeping the electronics on the deck.

The transmit voltage response (TVR) of the sound source is verified as shown in Figure 2.2. The testing was accomplished in a 1 m^3 tub, which limited the resolution of the calibration. Nonetheless, a coarse frequency response has been obtained. As can be observed, there is a degradation in the bandwidth of the transducer (the manufacturer bandwidth is over 5 kHz, while the measured bandwidth is closer to 2.5 kHz) and this is attributed to the poor match between the PA output and the transducer.

3.2 Deployments

The high flow conditions inherent to the tidal stream industry impede subsea wireless communication of data, through the high intensity of flow noise, the rapidly changing underwater communication channel conditions, and the susceptibility of equipment to mechanical stress and breakdown.The specific objectives of the proposed sea trial are 1) to test the MIMO communications system for medium to long range underwater acoustic communication in a point-to-point link, and 2) confirm the reliability and performance of multi receiver underwater acoustic communication system. 3) and analyze the MIMO communication channel for STBC communications.

In the the following two sections the deployments summary will be presented. First in 3.2.1, a deployment in the Northwest Arm, Halifax will be presented, then in 3.2.2, a deployment in Grand Passage, NS will be summarized.

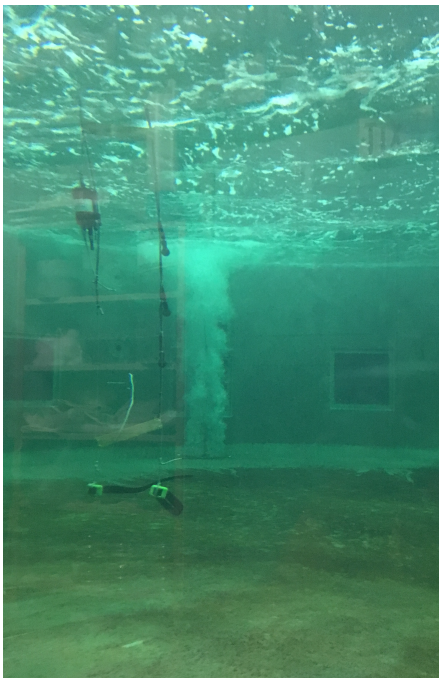

Figure 3.6: Deployment in Dalhousie aquatron

3.2.1 Deployment 1: Northwest Arm, Halifax

This experiment assessed the quality of a MIMO communication systems. A communication system is deployed over moderate range and the maximum range that we achieved is 1 km.

This experiment is performed near Dingle playground dock in Northwest arm, Halifax. The location of the moored receiver is approximately at 44° 37' 47.68" N, 63° 35' 36.46" W. The travelling distance between the Dingle playground dock and the final location in the arm is 1.08 US nm.

The transmitter ship was supplied by NWA Ferries as shown in Figure 3.8, and the receiver was deployed using a small dinghy. Note that an RF buoy was used to monitor the acoustic stream in real-time from the shore. In Figure 3.7, the approximate GPS location for the receiver and transmitter locations is overlaid over the satellite image provide by on Google Earth.

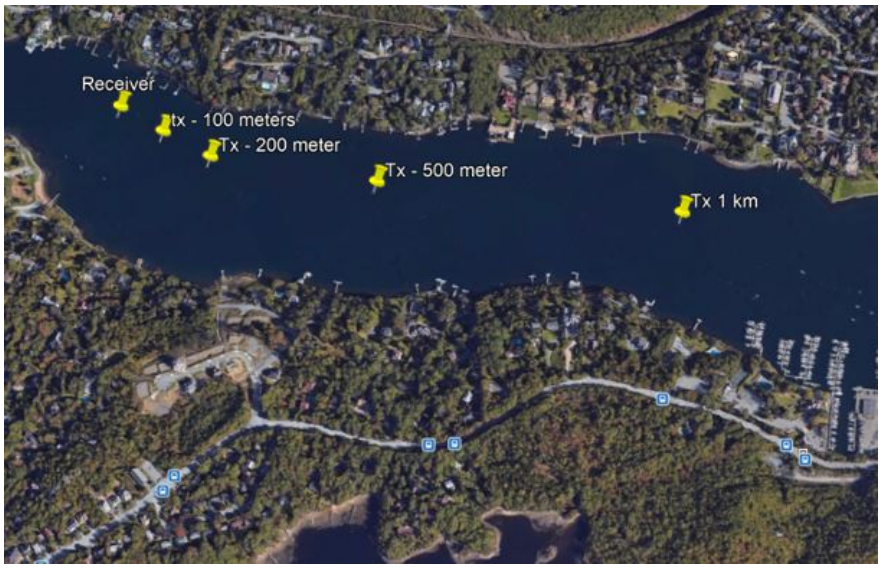

Figure 3.7: Dingle sea trail sensor placement

The vessel utilized for transmitter deployment was 8 m long, 2.7 m wide with a small enclosed wheel house, A 2000 W 120 V generator was used to drive the power amplifier, and for support equipment. GPS locations during the deployment were monitored.

For safety issues, and quality of measurements, the operations were limited to a narrow straight in the Arm, although there was a lot of pleasure boat activity near receiver bouy due to a nice summer day. The winds were very low, below 10 kph and the sea state was consist solely of a swell.

A cross-section of the deployment is shown in Figure 3.9 with representative dimensions. The receiver was anchored to the seabed, the primary acoustic receiver consists of a TR-ORCA with a five-hydrophone vertical line array (VLA). The wavelength at 27.5 kHz is

Figure 3.8: Side view of the NWA boat in northwest arm, Halifax

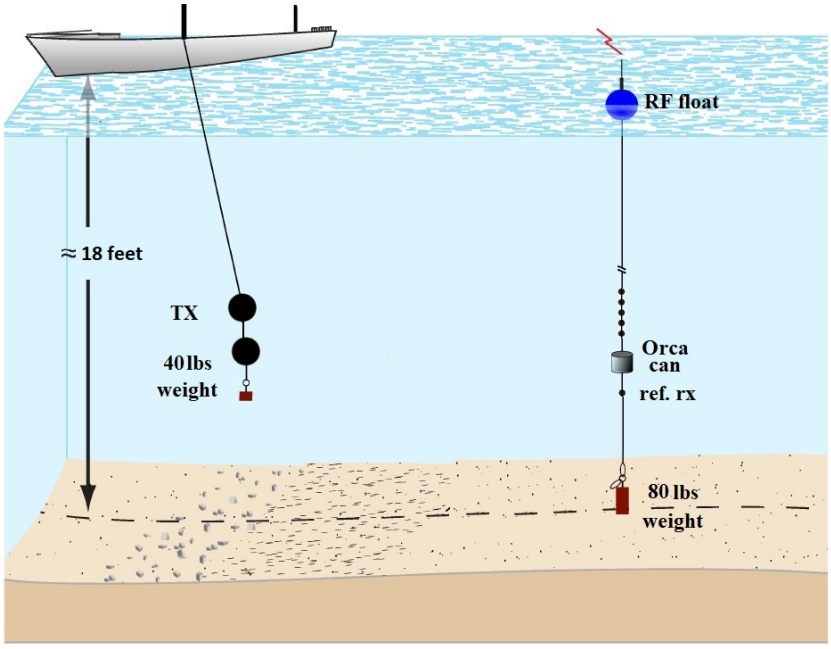

Figure 3.9: Depiction of receiver deployment in Northwest Arm, Halifax

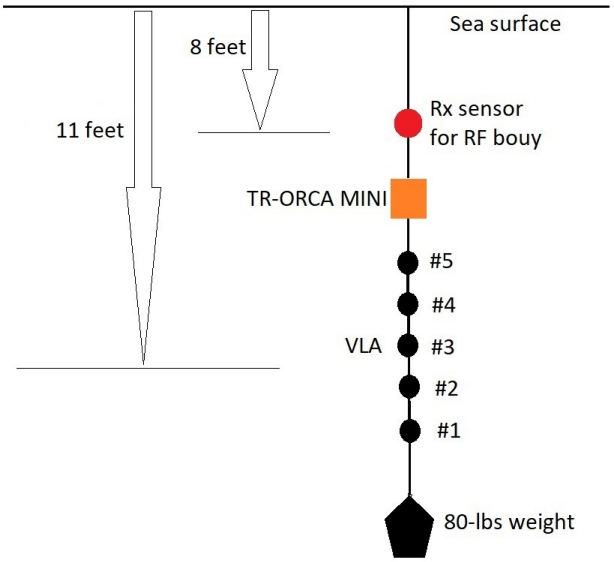

Figure 3.10: Deployment of the receiver equipment in Northwest Arm, Halifax

5.8 cm. The VLA inter-element spacing was more than 15 cm, more than the $\lambda/2$ at the center frequency of the acoustic operating band. The VLA depth was approximately 3.5 meters from the surface of the water. A pictorial description is provided in the Figure 3.10. It was anchored to the seabed using 80 pounds of weight and had no surface expression. The receiver distance from the seabed remained very stable throughout the experiment. Transmitter separation between the elements was about 1.5 meter, it was deployed from the side of the boat using a 5 meter rope. It was manually deployed and pulled out of water at each station and a 40 pound weight was used to stabilise the two sound sources.

To test the communication link at different ranges, the boat was anchored at predefined GPS locations and the transmitter was deployed from the vessel. The GPS position recorded are reported in Table 3.1. The transmitter was deployed for each station at a depth of about 3.5 meters. The depth of the transmitter was bound by the cable connecting sound sources to the power amplifier(PA).

To supply the signal, the transmitter electronics and PA were installed inside the wheel house. For each range, a set of pre-defined wave-forms were loaded and played using the FPGA. The output was fed to the PA through the internal sound card. The output RMS voltage of 10.5 V_{RMS} was generated using the PA. Note that a multi-meter was used to monitor the output Voltage. The operation was performed with high level of safety using

	Latitude	Longitude
Receiver	44°37'47.68"N	63°35'36.46"W
Transmitter @ 100m	44°37'44"N	63°35'35"W
Transmitter @ 200m	44°37'40"N	63°34'25"W
Transmitter @ 500m	44°37'36"N	63°35'21"W
Transmitter @ 1km	44°37'30"N	63°35'06"W

Table 3.1: GPS location of actual deployment stations in Northwest arm

a plastic box as shown in Figure 3.11 and precautions were taken to avoid any electrical hazards.

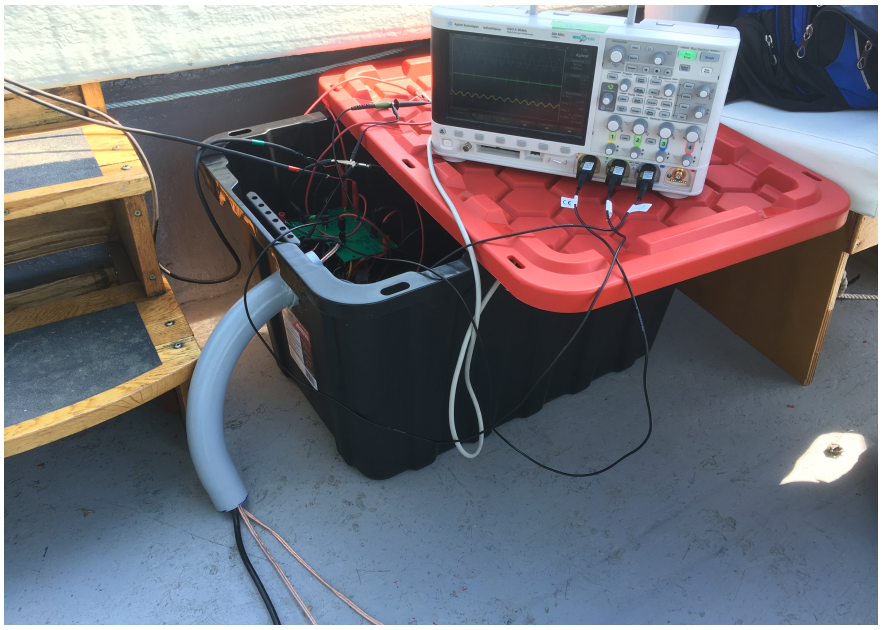

Figure 3.11: Electronics box for transmitter

To transmit the communication waveforms, wavefiles were generated from the FPGA. The FPGA was controlled by the GUI using the transmit laptop, amplified to the appropriate level, and applied to the transmit sound source. Each wavefile was played for each deployment setup. For each transmit station, the sound source was deployed from the transmit vessel at a depth of 3.5 meters. This was repeated at each transmit station. The power supply produced 40 Vdc. To make sure that the signal stays linear and stable, the FPGA output amplitude was adjusted for each modulation type (between 0 % and 100%). The power amplifier maximum input peak to peak voltage was 2 V_{PP}.

At each station, the following communication waveforms were transmitted :

- The STBC combined with PSK, QPSK, 16 PSK @ 5 baud. A transmission duration of 3.3 minutes for each modulation order allows the transmission of 1 million symbols.
- The STBC combined with FSK, 2-FSK, @ 78 baud. A transmission period of 3.3 minutes each modulation order allows for the transmission of 25000 symbols.
- FSK without MIMO, @ 78 baud. The transmit time of 5.4 minutes for each modulation order allows for the transmission of 25000 symbols.

3.2.2 Deployment 2: Bay of Fundy, Parrsboro, NS

Similarly, another sea trial was performed in the Bay of Fundy, near Long Island Nova Scotia. The geographical area is known for high flow noise and largest tides in the world. The receiver was deployed at a greater depth and very high flow environment. A planned transmitter and receiver locations are summarized in Table 3.2. Note, the receiver was deployed in the bay of Fundy for an additional 7 days with a schedule consisting of 12 hours on followed by 24 hours off to record marine mammal activity.

	Latitude	Longitude
Receiver	44°18'28.42" N	66°20'36.76"W
Transmitter @ 100m	44°17'28.90"N	66°20'31.15"W
Transmitter @ 200m	44°17'33.59"N	66°20'31.11"W

Table 3.2: Location of deployed receiver and multiple transmitter stations in Bay of Fundy

The vessel shown in Figure 3.12 was a Northumberland hull Cape Islander, 12 m long, 3.7 m wide with a small enclosed wheel house. A 2000 W 120 V generator was used to drive the power amplifier, and for support equipment. GPS locations during the deployment were monitored by the boat captain. A hoist installed on the vessel was also used during deployment and recovery of equipment.

The procedure used to deploy the transmitter was same as Northwest Arm but the receiver deployment was different. Instead of deploying it in the middle of the water column, it was deployed on the sea floor using a cage as shown in the Figure 3.13.

The primary acoustic receiver consists of a TR-ORCA with a five-hydrophone horizontal array (HA) as shown in Figure 3.14. An acoustic receiver (TR-ORCA) was attached to the bottom frame positioned on the seabed. The HA inter-element spacing was 18 cm, which is equal to the 3 λ at the center frequency of the acoustic operating band. The HA depth was

Figure 3.12: Overhead picture of boat used in the deployment

approximately 25 meter from the surface. It was anchored to the seabed using 80 pounds of weight and has no surface expression. An acoustic release can also be seen in the Figure 3.13. The wind was very high on the day of testing approximately 16-24 kph with a sea state between 2 and 3. There were huge swells while testing at 200 m station. Two narrowband transducers (27.5 kHz) were used to transmit acoustic energy with each transducer being capable of delivering up to 178 dB re 1uPa @ 1 m of energy. When both transducers were operating together, 125 dB re 1uPa @ 1 m was emitted into the marine environment. Trials were run for seven days but, the active acoustic transmissions only occurred on days 1, while passive acoustic data recordings occurred for the remainder of the trial to capture marine mammal activities in the area.

Note that to ensure that marine mammals present in the area remained unharmed from the active source transmission, a mitigation plan was submitted and approved by the Department of Fisheries and Oceans Canada.

The pair of experiments that were performed in this work to assess the performance of the communication system are 1): the characterization of the time-variant underwater acoustic

Figure 3.13: Cage used to deploy receiver at the Fundy Ocean bed

channel properties and, 2) the evaluation of a highly reliable STBC Alamouti modulation technique for co- existing channels such as underwater communication channel. Next, in Section 3.3 the channel characteristics will be presented, while the performance of the measured STBC will be described in Chapter 4.

3.3 Channel Characterizations

In this section, the channel statistical characteristics will be evaluated both in the Halifax Northwest arm, and in Grand Passage.

To obtain the 2×5 MIMO spatial channel impulse response as a function of time, a 4095-chip PRN sequence is transmitted. Multiple PRN sequences are transmitted to obtain several consecutive channel impulse responses. Since the symbol rate is 5000 bits per second, the channel impulse response resolution is 1/5000. Since the duration of each PRN sequence is $4095/5000 = 0.8$ sec, a sequence of channel impulse responses are produced at a rate of 1.2 Hz.

As an example, Figure 3.15 shows the output of the cross-correlation operation to recover the two channels between the two projectors, and the receiver for the 100-meter deployment in the Halifax NWA. Since the PRN signature is delayed by 600 symbols on transmit projector 2 with respect to transmit projector 1, at the receiver, the separation between the two channel impulse responses is $\Delta_{CIR} = 600/5000 = 120$ msec. This allows to obtain $h_{11}(t, \tau)$ between

Figure 3.14: Horizontally mounted hydrophone array

transmit element #1 and receive element #1 as well as $h_{21}(t, \tau)$ between transmit element #2 and receive element #1. By repeating the procedure for all receivers, a 2×5 MIMO spatial channel impulse response can be characterized.

Using the channel impulse response, different statistics can be extrapolated: in this work, the transmission loss, the delay spread, the spatial correlation as well as the SNR are obtained.

The transmission loss is obtained by integrating the channel impulse response over all the path delays. For example, the transmission loss for the 100-meter scenario is shown in Figure 3.16 for a 400-second window.

To represent the severity of the multipath channel, the RMS delay spread defined in Section 2.1.2 is evaluated as a function of time. Its average over time is summarized in Table 3.3.

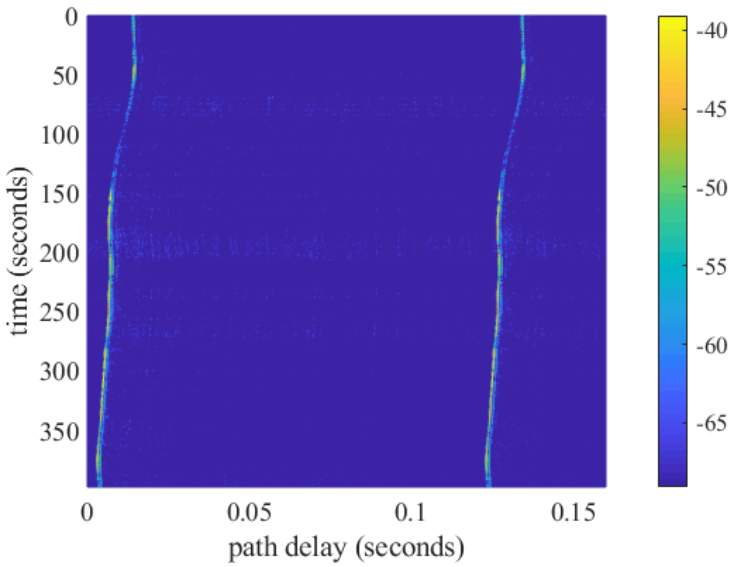

Figure 3.15: Impulse response between two projectors and one receiver for 100 meter separation in the Halifax Arm.

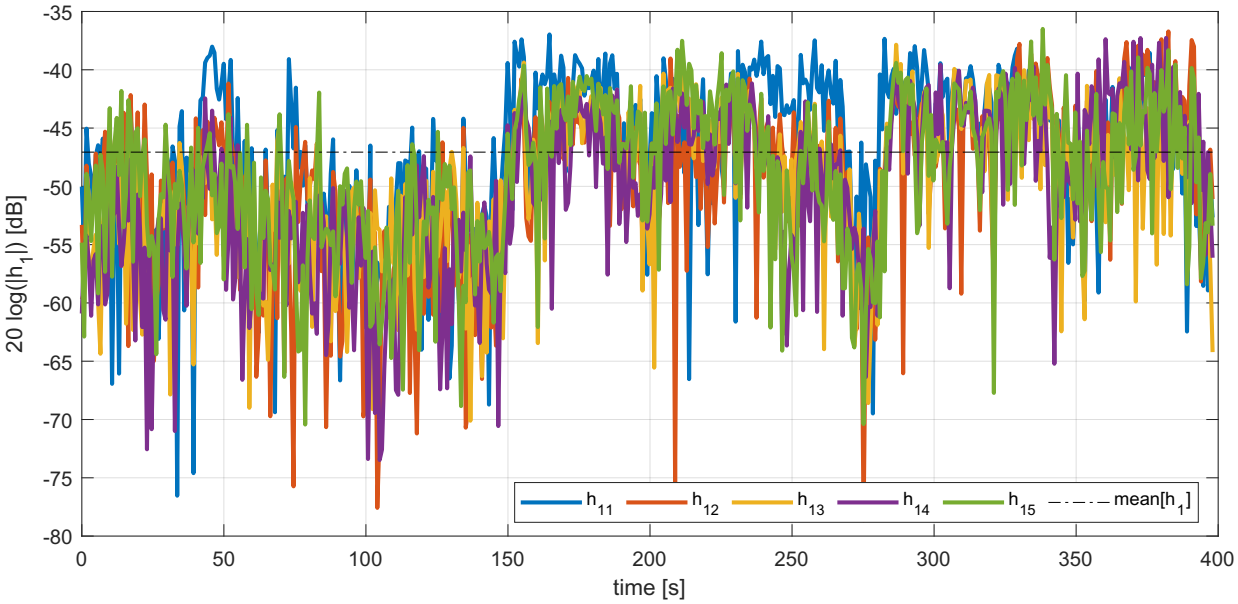

Figure 3.16: Transmission loss between the transmitter 1 and all hydrophones for 100 meter separation in the Halifax Arm.

To obtain the mean spatial correlation between pairs of hydrophones, the measured cross-correlation matrix R_{NN} can also be calculated. Specifically, between hydrophones a, and b, the value of the cross-correlation matrix between signal y_a and y_b at index (a, b) is

$$R_{NN}(a,b) = \frac{\sum_{i=1}^{N}(y_{a,i} - \overline{y_a})(y_{b,i} - \overline{y_b})}{\left(\sum_{i=1}^{N}(y_{a,i} - \overline{y_a})^2(y_{b,i} - \overline{y_b})^2\right)^{0.5}}$$

Then, the average spatial correlation between adjacent hydrophones is obtained by averaging over the adjacent elements of the R_{NN} matrix. The results of the spatial correlation between pairs of receive hydrophones is summarized in Table 3.3.

Table 3.3: Measured Channel Characteristics in Halifax North West Arm

	Transmission Loss (dB)	Delay Spread (msec)	Spatial Correlation
100 meters	-47.5	3.0	0.66
200 meters	-71.1	2.0	0.71
500 meters	-85.4	4.5	0.46
1000 meters	-102.4	7.8	0.43

For the Halifax deployment, the TL does not follow the spherical spreading law. Additional loss could be due to the absorption, as well as loss of cross-correlation gain when the channel is subject to time variation. Note that the Doppler spread and the delay spread increases as the distance between transmitter and receiver increases. The spatial correlation decreases with increase in the distance, although it is still quite high.

For the Grand Passage deployment, for the 100 meter deployment the SNR is on the order of 31 dB, and is calculated by using a noise power measurement before transmission. Similarly, for the 200 meter deployment the SNR is on the order of 34 dB. It should be noted that the flow noise power at the hydrophones was significant, particularly for the 100 meter deployment. While the flow noise is away from the communication band, its high power drove the hydrophones into saturation, this entirely corrupting the signal received for the 100 meter data.

Table 3.4: Measured Channel Characteristics in Grand Passage, Nova Scotia

	Gain (dB)	Delay Spread (msec)	Spatial Correlation
200 meters	-24.8	4.0	0.65

Chapter 4

Evaluation of Receiver Reliability

In this chapter, the post processing of the results and the evaluation of the receiver performance will be presented. In Section 4.1, the methodology followed to extract data from the wave files and signal processing techniques will be explained. Section 4.2 will present the simulation results and the discussion on the receiver performance.

4.1 Signal Processing

In this section signal processing methods will be explained.

The data was post-processed following the experiments. The first step of the data analysis was accomplished using the free, open source, digital audio editor known as Audacity. To make sure that the correct form of modulation is decoded a visual comparison of the data burst with the log book entry is performed. The individual wavefiles were extracted visually from Audacity. As shown in Figure 4.1 data is a sample of 1 recorded channel represented on a spectrograph. Pulses are the 6 minute long wavefiles with a center frequency of 27.5 kHz. Figure 4.2 shows the end and start of two sequential waveforms. It can be seen from the Figure 4.2 that there are multipath echoes following the end of transmission. A long wait period ensured the echoes were negligible before the next transmission. To assist in proper extraction of the received wavefile, audio cues can also be heard to realize the end of transmission.

It was found through observation on every wavefile that was isolated that the duration of the received waveform was not exactly complete frames. The start and stop of the transmission of wavefile does not gurantee the start and end of frame. This is due to that fact that FPGA repeat a PN sequence after every 4095 bits. Start and stop of the transmission of wavefile does not guarantee that it start from the 1st bit and end at the 4095 bit. Doppler shift and spread dilating are other two reason for errors.

The first step of decoding data comprise of resampling to 75000. The sampling rate of pressure case is 384 ksps and reducing it to lower number allow a better data decoding.

Following the resampling of the waveforms, they are now suitable for proper demodulation and decoding. During the trials in the North West Arm sea trials, the FSK algorithm was designed to have a symbol period of 0.0128 seconds and were transmitted at 100m, 200, 500 and 1 km. The purpose of the symbol time of 0.0128 seconds allows the analysis of symbol length on performance and to stop and intersymbol interference. This exact scheme was transmitted at various distance in Halifax NWA and Grand Passage at two different days. It is important to mention here that the receiver was a vertical line array in the NWA and while it was horizontal array in the Bay of Fundy. The separation between the receiver elements was more than $\lambda/4$ in both arrangements. To summarize the two day transmission: Day 1 in NWA, sent approximately six minutes wavefile at 100m, 200m, 500m and 1km. Day 2 in the Bay of Fundy sent approximately six minutes wavefile at 100m and 200m.

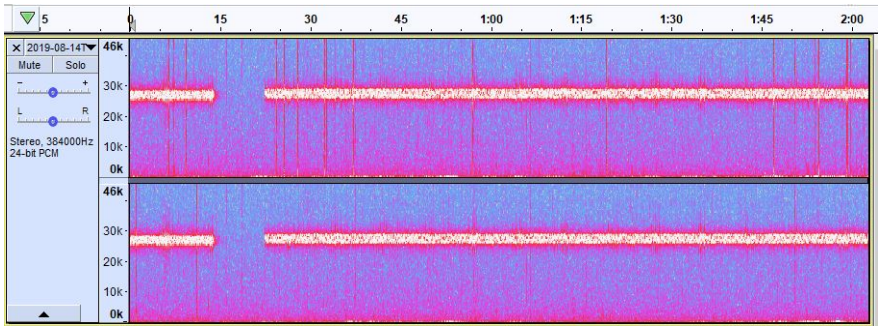

Figure 4.1: Sample data Audacity screen shot

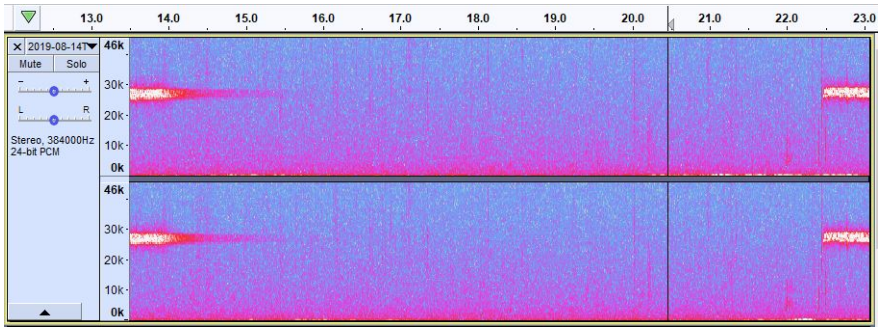

Figure 4.2: Audacity screenshot showing ecohes at the end of transmission

4.2 Simulations and Performance Discussion

In this section, the simulations for various modulation schemes under different channel parameters to obtain the BER curves is performed and analysed. Additionally performance

of the multi-channel FSK is discussed. Models of the transmitter, wireless channel, and receiver are implemented with MATLAB. The procedure consists in providing simple, yet realistic, subsea conditions through an iterative and incremental design procedure. For the purposes of the simulation, 5 decoder iterations were used. First, to confirm the validity of the model, the BER is evaluated in controlled conditions and compared against a known theoretical performance in AWGN conditions. Secondly, the impact of multipath arrival is evaluated using channel impulse response shown in Figure 4.3(b). The effect of multipath creates multiple versions of the same symbols and they arrive at receiver with exponential delay. Destructive interference degrades the received signal strength. As such, the model now represents a static multipath ocean environment.

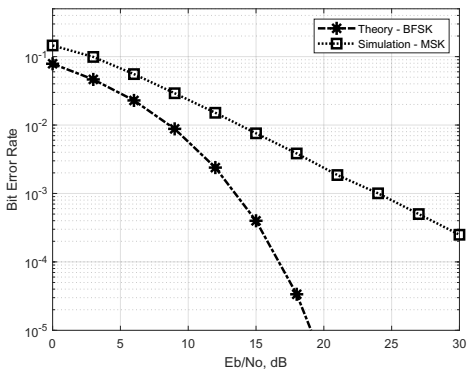

(a) Bit error probabilty curve for MSK modulation

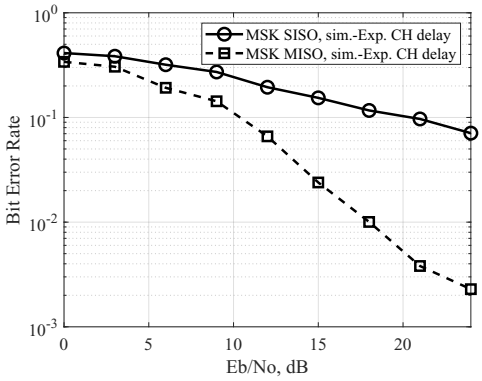

(b) Multi-path - exponential channel delay

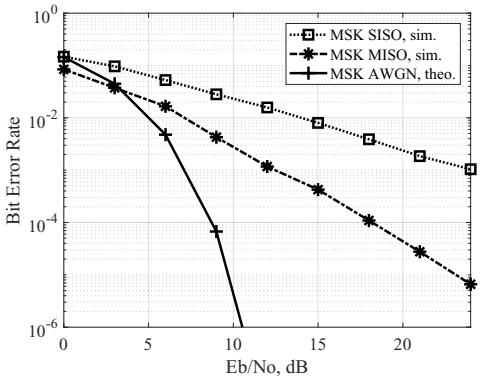

(c) Flat fading conditions

Figure 4.3: Simulation of CPFSK(h = 1/2, MSK)

Figure 4.3 shows the BER of MSK modulation in an AWGN, exponetial channel delay

and MISO implementations theoretical performance. Observe the reliability degradation due to the introduction to multipath in exponentially decaying channel for a 78-bps symbol rate. This deterioration is due to the non-coherent addition of multipath arrivals, which causes channel amplitude fading. During the simulation, 4095-symbol frames are transmitted for a total bit count of approximately 25,000,000 bits.

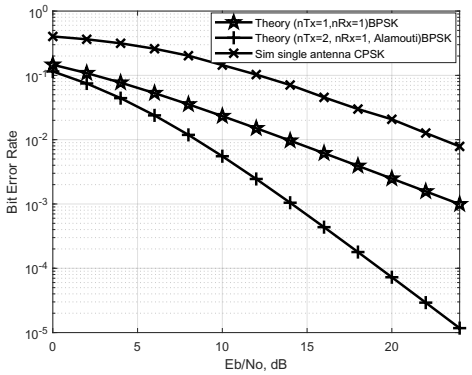

(a) CPFSK simulation single Tx and Rx

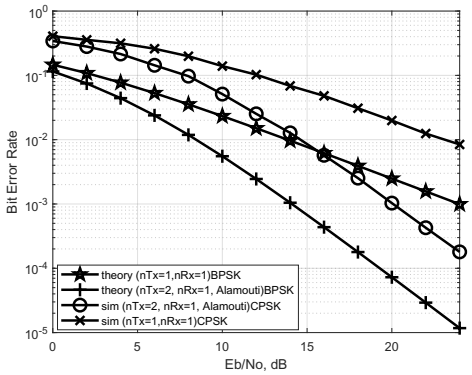

(b) Simulation of the combine analysis of CPFSK and BPSK

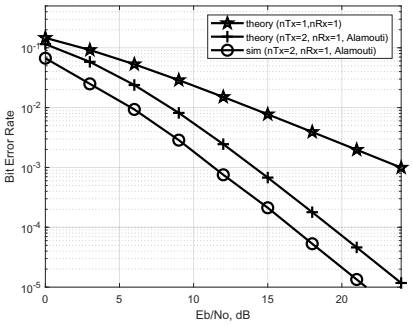

(c) Simulation of BPSK Alamouti

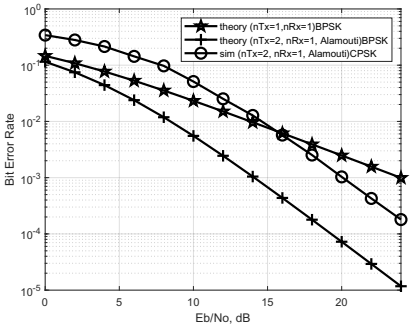

(d) Simulation of CPFSK Alamouti

Figure 4.4: Simulation of CPFSK(h = 30)

However, when comparing the MSK SISO BER results with the MSK MISO BER results in a Rayleigh fading channel, a degradation in performance is seen, as shown in Figure 4.3(c). This performance degradation is due to a difference in number of receive antennas. To achieve a comparable BER performance of 10^{-5} with SISO MSK system, 5 dB more signal power is required. Observing the multipath performances in Figure 4.3(b), MISO offer better performance to obtain the same order of BER at much lower SNR.

One can conclude from the initial simulation that the effect of steady-state flat fading

deteriorates the system significantly. Further work needs to be done to improve the performance in a harsh multipath environment.

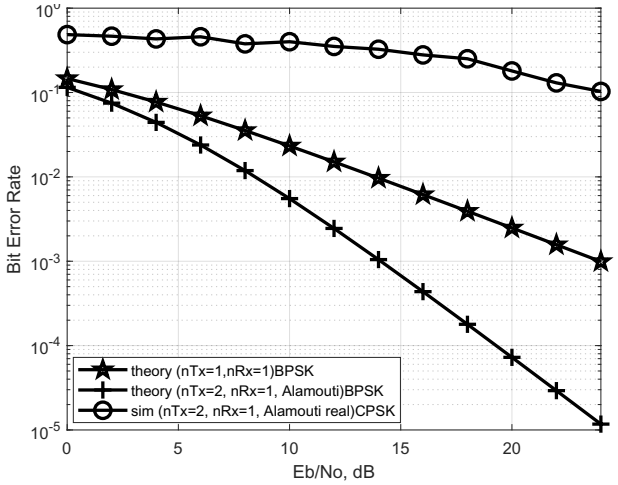

Figure 4.5: CPFSK Alamouti with channel coefficient from Bay of Fundy

Figure 4.4 provides details about the simulated probability of bit error for CPFSK as a function of SNR for different conditions. First, in Figure 4.4(a), the BPSK with STBC is compared with BPSK and CPFSK single-input single-output (SISO) in flat fading conditions, assuming a Rayleigh fading channel. The diversity gain is clearly observed in comparison to a SISO scenario. In Figure 4.4(c), the performance of the BPSK STBC code, in multipath conditions is also evaluated. Similarly in Figure 4.4(d), CPFSK with Alamouti STBC is compared to BPSK with Alamouti code. It is understood for the curves that CPFSK with STBC is comparable to BPSK with added benefit of FSK resilient to Doppler shift. A combined analysis is shown in Figure 4.4(b). The results demonstrate that the STBC also provides improvement in performance in multipath conditions. The improvements in BER due to the implementation of Alamouti code provides a usable and reliable communication algorithm for FSK modulation schemes.To further improve the performance, a MIMO STBC can be easily implemented with the prototyping system available. Error correction codes, such as Turbo codes can further improve the performance.

STBC vastly improves the performance of communication channel such as Rayleigh as depicted by the simulations above, underwater communication channel is an upcoming area of research. During sea trail multiple sources were deployed and channel information was deduced for the data. Figure 4.5 depict the performance of Alamouti code in a high flow, highly correlated Bay of Fundy channel.

It is evident from the result that STBC preform considerably low in channel with high co-relation. The separation of the sound sources was much greater than 10 λ, even then STBC gains were not evident.

In the following few paragraphs the system performance is presented and analysed. Table 4.1 shows the BER after demodulation for 2-FSK for each hydrophone channel. The BER results for BPSK is shown in Table 4.2 for comparison purpose. Missing slots in the BPSK rows indicates the loss of data due to the excessive noise in the channel while transmitting the waveform. The result shown by the BPSK is comparatively better than FSK, presence of ambient noise during the transmission of wave file could be one of the prominent reason.

Table 4.1: Measured BER Northwest Arm, Halifax 2-FSK

Distance		100 meters	200 meters	500 meters	1 kilometer
Bit error rate - CPFSK with two transmitters					
Number of receivers	1	0.02	0.08	0.13	0.29
	2	0.0044	0.0560	0.0889	0.2767
	3	0.0023	0.0447	0.0752	0.2628
	4	0.0013	0.0436	0.0531	0.2496
	5	6.3e-04	0.0400	0.0471	0.2479

Table 4.2: Measured BER Northwest Arm, Halifax BPSK

Distance		100 meters	200 meters	500 meters	1 kilometer
Bit error rate - BPSK with one receiver					
Number of transmitters	1	-	0.07	-	0.17
	2	9.1e-3	3.9e-4	0.03	0.31

The bit error ratio (BER) measured for 2-FSK observed an average BER of 0.005726 for 100 m, 0.05286 m for 200 m, 0.07886 for 500 m, and 0.2654 for 1 km. Comparatively the BER for 4-BFSK as shown in Table 4.3 with observed average values of 0 for 100 m, .002341 for 200 m, 0.01687 for 500 m, .34568 for 1 km. Note that, a part of 100m 4-FSK data sequence was lost due to a malfunction in the storage unit and only 1514 bits were received. There were no bit in error for the 1514 bits received. It is very evident from the results that the addition of multiple receive hydrophones drastically improved the BER of the system resulting in minimal errors.

Table 4.3: Measured BER Northwest Arm, Halifax 4-FSK

Distance		100 meters	200 meters	500 meters	1 kilometer
Bit error rate - CPFSK with two transmitters					
Number of receivers	1	0.0	0.0114	0.0516	0.3650
	2	0.0	3.05e-04	0.0212	0.3535
	3	0.0	0.0	0.0106	0.3438
	4	0.0	0.0	0.00038	0.3359
	5	0.0	0.0	0.976e-04	0.3347

From the bit error rate tables, one can observe the performance degradation due to the greater distance. Although there is degradation while using 5 receiver, but performance is superior than using only single antenna. This degradation occurred because of the multipath delay spread. The boat activity in the Northwest arm during 4-FSK was less than that of 2-FSK resulting in a less ambient noise and other signal deteriorating effects. As a result, the performance was significantly better than that of 2-FSK at 100 m transmission. Two definitive points can be drawn from this 1) that increase in boat activity around communication system increases the number of bit errors, hence underwater communication is time sensitive and 2) degradation in performance correlates with increased communication distance.

Table 4.4: Measured BER bay of Fundy 2 FSK

Distance		100 meters	200 meters
Bit error rate - CPFSK with one transmitter			
Number of receivers	1	0.2931	0.1369
	2	0.1676	0.1089
	3	0.1503	0.0924
	4	0.1449	0.0861
	5	0.1280	0.0833

Furthermore, Sea trial results from Bay of Fundy are presented Table 4.4 and Table 4.5. The receiver was deployed with horizontal array in comparison to a vertical array in Dingle, also the deployment was in high flow environment.

Due to the very high flow noise the receiver was saturated during the transmission at 100 m. Hence, a comparison between the results at 100 m and 200m shows a degraded performance at 100 m station. For 200 m data, the results show comparably identical BER

Table 4.5: Measured BER bay of Fundy 4 FSK

Distance		100 meters	200 meters
Bit error rate - CPFSK with one transmitter			
Number of receivers	1	0.3913	0.1589
	2	0.3464	0.1432
	3	0.3362	0.1287
	4	0.3310	0.1100
	5	0.3250	0.1087

performance as the Dingle sea trial.

The bit error ratio (BER) measured for 2-FSK observed an average BER of 0.1767 for 100 m and 0.1015 for 200 m respectively. Comparatively the BER for 4-BFSK as shown in Table 4.3 with observed average values of 0.34598 for 100 m and 0.1299 for 200 m.

Comparing the results from Tables 4.1 and 4.3 with the bit error ratio from Tables 4.4 and 4.5, respectively, one confirms the correlation between degradation in confidence with increase in bit errors. It is also shown that with increasing distance, system performance degrades.

Chapter 5

Conclusion

In this chapter, the thesis contributions are summarized. Specifically, Section 5.1 outlines the major contributions of this work. Section 5.2 discusses the potential future work.

5.1 Summary of Contributions

In this work, an underwater acoustic link was designed, analyzed modeled, and then tested in realistic conditions.

The research in this thesis describes a design methodology for non-coherent communication modulation schemes in high interference environments. Firstly, the development of a transmitter on an Xilinx FPGA is presented in this work. Secondly, multiple deployments with different array configurations in realistic environments were achieved. An STBC code was tested using a real channel and the performance of FSK coded MIMO was analyzed. Finally, the signal processing accomplished at the physical layer for post processing of the data to demonstrate a reliable SDAM was accomplished.

Two low-data rate waveforms, 2-FSK and 4-FSK, were implemented to achieve high reliability at a range close 1 km underwater in two very different environments. The addition of multiple receivers greatly increases the robustness of both FSK modulation schemes to usable performances, since diversity gain can be obtained.

Results presented in this work strongly suggest that a multiple receiver array can significantly improve the performance. Additionally, the Alamouti STBC coded FSK in non-correlated underwater communication channel can provide additional performance both in terms of diversity and capacity.

The performance of the system was also characterized in controlled environments. Specifically, 2-FSK and 4-FSK achieved, respectively, an average BER of 0.130 and 0.0516 for 500 meters the NWA, using the receiver in the VLA configuration. Similarly, the performance in the Bay of Fundy deployment in a horizontal array configuration were presented. Although, it is demonstrated from STBC performance that even for a distance of 15 λ do not

provide significant for spatial diversity gain in the proposed scenario, the use of alternative techniques to maintain low cross-correlation between the elements can potentially improve the performance.

5.2 Future Work

The future research related to this work includes improving the STBC. For example, the use of Alamouti code over 3 or 4 sound sources may improve robustness, which is important for diversity gain at high speed. Identification of the specific conditions to decrease the spatial correlation would have to be studied and the implementation of a multi-sources transmitter using the described modulation techniques realized, simulated, and tested. A sea trial procedure for a network deployment with multiple sources and hydrophones is drastically more involved than a point-to-point link deployment, but an interesting scenario to look at.

Other future research directions include a further study of more complex STBC codes beyond simple yet powerful Alamouti code, studying and deducing a synchronization mechanism to ease the signal processing at the receiver and design towards a fully autonomous, re-configurable SDAM optimized using coherent detection. The study of the performance on specific packet length, and optimizing the number of receivers to maximize the decoder efficiency and performance is also important. Finally, incorporating frame packet design to mitigate channel impairments, such as a guard interval, may also be studied.

Bibliography

[1] K. Domrese, A. Szajna, S. Zhou, and J. Cui, "Comparison Of The Ranging Function Of Three Types Of Underwater Acoustic Modems," in *2014 IEEE 11th International Conference On Mobile Ad Hoc And Sensor Systems*, 2014, pp. 743–748.

[2] I. F. Akyildiz, D. Pompili, and T. Melodia, "Underwater Acoustic Sensor Networks: Research Challenges," *Ad Hoc Networks*, vol. 3, no. 3, pp. 257 – 279, 2005. [Online]. Available: http://www.sciencedirect.com/science/article/pii/S1570870505000168

[3] R. K. Moore, "Radio Communication In The Sea," *IEEE Spectrum*, vol. 4, no. 11, pp. 42–51, 1967.

[4] H. S. Dol, P. Casari, T. van der Zwan, and R. Otnes, "Software-Defined Underwater Acoustic Modems: Historical Review And The NILUS Approach," *IEEE Journal Of Oceanic Engineering*, vol. 42, no. 3, pp. 722–737, July 2017.

[5] X. Hu, D. Wang, Y. Lin, W. Su, Y. Xie, and L. Liu, "Multi-Channel Time Frequency Shift Keying In Underwater Acoustic Communication," *Applied Acoustics*, vol. 103, pp. 54–63, 02 2016.

[6] G. Singh and A. Kumar, "Study Of Various Space Time Codes For MIMO Systems," in *2015 IEEE International Conference On Computational Intelligence Communication Technology*, Feb 2015, pp. 604–607.

[7] J. Yu and Y. Lin, "Comments On Semi-Blind Channel Estimation And Equalization For MIMO Space - Time Coded OFDM," *IEEE Transactions On Circuits And Systems I: Regular Papers*, vol. 55, no. 11, pp. 3513–3513, Dec 2008.

[8] G. Ganesan and P. Stoica, "Space-Time Block Codes: A Maximum SNR Approach," *IEEE Transactions On Information Theory*, vol. 47, no. 4, pp. 1650–1656, May 2001.

[9] S. M. Razavi and H. Zamiri-Jafarian, "Joint Subspace Beamforming And Space-Time Coding In Wireless MIMO Systems," in *2009 International Conference On Advanced Technologies For Communications*, Oct 2009, pp. 99–103.

[10] I. J. Youn, "Noncoherent M-ary Orthogonal FSK Alamouti Space-Time Coding With Antenna Selection," in *2008 10th International Conference On Advanced Communication Technology*, vol. 1, Feb 2008, pp. 723–730.

[11] R. Urick, *Principles Of Underwater Sound*. Peninsula Publishing, 2013. [Online]. Available: https://books.google.ca/books?id=UzpVrgEACAAJ

[12] A. A. Dobbin, "Reliable acoustic link using non-coherent turbo-coded fsk," Ph.D. dissertation, Dalhousie University, 2018. [Online]. Available: https://dalspace.library.dal.ca/handle/10222/73919

[13] M. Kim, T. Lee, T. Im, and H. Ko, "The Analysis Of Coherence Bandwidth And Coherence Time For Underwater Channel Environments Using Experimental Data In The West Sea, Korea," in *OCEANS 2016 - Shanghai*, 2016, pp. 1–4.

[14] Proakis, *Digital Communications 5th Edition*. McGraw Hill, 2007.

[15] D. Tse and P. Viswanath, *Fundamentals Of Wireless Communication*. USA: Cambridge University Press, 2005.

[16] S. M. Alamouti, "A Simple Transmit Diversity Technique For Wireless Communications," *IEEE J. Select. Areas Comm.*, vol. 16, no. 8, pp. 1451–1458, Oct 1998.

[17] A. Wittneben, "Base Station Modulation Diversity For Digital Simulcast," in *[1991 Proceedings] 41st IEEE Vehicular Technology Conference*, May 1991, pp. 848–853.

[18] ——, "A New Bandwidth Efficient Transmit Antenna Modulation Diversity Scheme For Linear Digital Modulation," in *Proceedings Of ICC '93 - IEEE International Conference On Communications*, vol. 3, May 1993, pp. 1630–1634 vol.3.

[19] N. Seshadri and J. H. Winters, "Two Signaling Schemes For Improving The Error Performance Of Frequency-Division-Duplex (FDD) Transmission Systems Using Transmitter Antenna Diversity," in *IEEE 43rd Vehicular Technology Conference*, May 1993, pp. 508–511.

[20] J. H. Winters, "The Diversity Gain Of Transmit Diversity In Wireless Systems With Rayleigh Fading," in *Proceedings Of ICC/SUPERCOMM'94 - 1994 International Conference On Communications*, May 1994, pp. 1121–1125 vol.2.

[21] W. H. Gerstacker and Others, "Equalization Concepts For Alamouti's Space-Time Block Code," *IEEE Trans. Comm.*, vol. 52, no. 7, pp. 1178–1190, July 2004.

[22] C. Bowick, C. Ajluni, and J. Blyler, *RF Circuit Design, Second Edition*, 2nd ed. USA: Newnes, 2007.

Appendix A

Personnel at Sea

A.0.1 Bay of Fundy, Nova Scotia

- Jean-Francois Bousquet (Scientist-in-Charge as well as communications system lead)
- Surinder Singh (Signal processing, Transmitter)
- Cole Ferguson (Transmitter)
- Richard Cheel (Marine Operations)
- Greg Trowse (Marine Operations)
- Gavin (Deployment)

A.0.2 Bay of Fundy, Nova Scotia

- Jean-Francois Bousquet (Scientist-in-Charge as well as communications system lead)
- Surinder Singh (Signal processing, Transmitter)
- Cole Ferguson (Receiver deployment)
- Adam Forget (Logs)
- Jeff Macdonald (Receiver)
- Mark Crispo (Transmitter handling)

Appendix B

Equipment Used in Bay of Fundy

- Transmitter System
  - Benthowave acoustic Projects
  - Benthowave BII-7522 power amplifier
  - Xilinx FPGA
  - Extension cable for power supply
  - High power cables to connect to/from PA
  - 110-V 2000-W Power Generator (SOAR/NWA)
  - UPS
  - Panasonic Toughbook with required software (Audacity, Matlab, TRAC)
  - Signal cable to extend the projector depth
  - 1 15-kg weights for the transmitter
  - 2 Multimeters
- Receiver Array
  - TR-ORCA with replenished batteries
  - Collar float
  - Hydrophone vertical and horizontal linear array
  - Acoustic release
  - Acoustic links
  - 5 meter nylon between anchor and acoustic release
  - 40-meter 3-strand Dyneema cable
  - Twine to attach acoustic link

  - 200-lbs weight
  - Receiver cage (Oceanography department Dalhousie)
  - End connectors to seal the case
  - Eye bolts and U bolt
  - 2 synthetic buoys
  - Reconfiguration cable
  - All end caps

- Monitoring System in Dingle
  - TR-ORCA-MINI with replenished batteries
  - TR-float with RF antenna
  - TR-float basestation
  - Omni antenna
  - 2 15-meter ethernet cables (green)
  - Asus laptop to reconfigure receivers
  - Monitoring hydrophone
  - 1 5-kg weights for the monitoring buoy
  - Mooring system (NWA ferries)
  - 2 synthetic buoys

- Support and Monitoring Equipment
  - Radios or cellphones
  - Tape measure
  - Scissors
  - Knife
  - Tie wraps
  - Sea sickness medicine
  - Sunscreen
  - Warm Jacket

Appendix C

Summary of experiments

Waveform	Objective	Tx time (minutes)	Max tx Power (dBm re 1 uPa @ 1m)
1) Single antenna (continuous wave)	fading channel	4	178
2) Multiple antennas (tones)	channel sounding	6.8	178
3) BPSK (without STBC, single channel)	channel sounding	6.6	187.5
4) BPSK (without STBC, multiple channels)	channel sounding	6.6	187.5
5) M-PSK (with STBC), for M = 1, M = 2, M=3	MIMO transmission	10	187.5
6) FSK (with STBC), for M = 1, M = 2	MIMO transmission	10.6	188
7) FSK (No STBC, 2-FSK, 4-FSK)	data transmission	10.6	178
8) LFM single channel	data transmission	5.34	178
Total time (minutes)		60.8	

Table C.1: Summary of experiments

	Latitude	Longitude
Receiver	44°37'47.68"N	63°35'36.46"W
Transmitter @ 100m	44°37'45.25"N	63°35'33.98"W
Transmitter @ 200m	44°37'7.74"N	63°34'22.75"W
Transmitter @ 500m	44°37'37.68"N	63°35'19.69"W
Transmitter @ 1km	44°37'29.45"N	63°34'58.37"W

Table C.2: Location of planned moored receiver and multiple transmitter stations in Northwest arm